

# A DPG method for Reissner–Mindlin plates <sup>\*</sup>

Thomas Führer<sup>†</sup>      Norbert Heuer<sup>†</sup>      Antti H. Niemi<sup>‡</sup>

## Abstract

We present a discontinuous Petrov–Galerkin (DPG) method with optimal test functions for the Reissner–Mindlin plate bending model. Our method is based on a variational formulation that utilizes a Helmholtz decomposition of the shear force. It produces approximations of the primitive variables and the bending moments. For any canonical selection of boundary conditions the method converges quasi-optimally. In the case of hard-clamped convex plates, we prove that the lowest-order scheme is locking free. Several numerical experiments confirm our results.

*AMS Subject Classification:* 74S05, 35J35, 65N30, 35J67, 74K20

## 1 Introduction

We present and analyze a discontinuous Petrov–Galerkin method with optimal test functions (DPG method) for the Reissner–Mindlin plate bending model. The model considers the influence of transverse shear deformations in the strain-displacement relations and may be viewed as a correction of the classical Kirchhoff–Love model. Most prominently, the effective shear forces and concentrated corner forces, that some scholars consider to be unnatural, are not needed in the Reissner–Mindlin model to reduce the number of independent edge reactions. While for thin isotropic plates the results of these models do not differ much, the more accurate kinematic assumptions of the Reissner–Mindlin model lead also to practical improvement of results for thick and orthotropic plates. On the other hand, principal advantages of the DPG framework are that it provides automatically stable approximations for any conforming discretization space [21, 22], and that adaptivity is a built-in feature, cf. [23, 19]. For mechanical models of thin structures, the framework can be used to construct formulations with the most relevant stress and displacement quantities of interest as primal variables. The underlying assumption is to have appropriate well-posed variational formulations with product test spaces. The construction of such formulations and suitable approximation spaces for the Reissner–Mindlin model is by no means trivial.

---

<sup>\*</sup>Supported by ANID (formerly CONICYT) through FONDECYT projects 1190009, 1210391

<sup>†</sup>Facultad de Matemáticas, Pontificia Universidad Católica de Chile, Avenida Vicuña Mackenna 4860, Santiago, Chile, email: {tofuehrer,nheuer}@mat.uc.cl

<sup>‡</sup>Civil Engineering Research Unit, Faculty of Technology, University of Oulu, Erkki Koiso-Kanttilan katu 5, 90570 Oulu, Finland, email: antti.niemi@oulu.fi

It should be noted that there is a long history of developing various other kinds of discretizations for the Reissner–Mindlin model, and there are several strategies to tackle the numerical phenomenon of transverse shear locking. Among them are, combined with mixed formulations, Helmholtz decompositions of the shear force [13, 3, 11], non-conforming approximations [3], and reduced integration [12, 14, 5], to name a few classical results. Some more recent approaches include special elements [2], weakly over-penalized discontinuous Galerkin methods [9, 10] and the DDR (discrete de Rham) complex method [24]. DPG schemes allow for very general meshes, see [7] for a non-conforming setup, similarly to virtual elements which have been developed for the Reissner–Mindlin model, see [8]. We also note that DPG schemes, being of minimum residual type, are related with least squares approaches. Such methods have been studied for a perturbed Stokes problem which behaves like the Reissner–Mindlin model, see [17, 16]. This list is far from being complete. For a more detailed discussion we refer to the recent paper [24] on the DDR method.

In the present paper, we continue our development of DPG schemes for plate and shell structures that started with the analysis of the Kirchhoff–Love plate model in [28]. Subsequently, we extended our techniques to the Reissner–Mindlin model [30] and shallow shells of Koiter type [29]. In both problems, Reissner–Mindlin plates and Koiter shells, different kinds of locking phenomena appear and it must be stressed that DPG schemes are not automatically locking free. In [29] we dealt with the membrane locking by increasing the approximation order of a trace variable. On the other hand, our previous Reissner–Mindlin plate study [30] focused on developing a variational formulation that converges to the Kirchhoff–Love case [28] when the plate thickness tends to zero. Whether that approach is locking free depends on the construction of discrete trace spaces, not considered in [30]. Let us also mention the study [18] of a DPG scheme for Reissner–Mindlin plates, though their analysis considers the plate thickness to be fixed.

Here, we complete the picture by utilizing a Helmholtz decomposition of the shear force (after suitable scaling), as proposed by Brezzi and Fortin [13] and thoroughly analyzed by Arnold and Falk in [3]. In this way, a variational formulation consists of three stages, the first to determine the irrotational component  $\nabla r$  of the scaled shear force  $\mathbf{q}$ , the second to determine the solenoidal component  $\mathbf{curl} p$  of  $\mathbf{q}$  together with other variables, and the third to recover the vertical deflection  $u$ . Stages one and three are simple Poisson problems which can be solved by standard finite elements, whereas stage two reflects the very Reissner–Mindlin model and is solved by a DPG scheme. Apart from variable  $p$ , it delivers the rotation field,  $\boldsymbol{\psi}$ , and the bending moments,  $\mathbf{M}$ , along with the artificial variable  $\boldsymbol{\eta} := t \mathbf{curl} p$  where  $t$  is the plate thickness.

Let us recall two important issues that determine the behavior of DPG approximations. First, optimal test functions are a theoretical construct and have to be discretized in practice. In order to maintain discrete stability, the existence of Fortin operators has to be shown, cf. [31]. For our Kirchhoff–Love setting from [28], this is done in [26]. In the case of the Reissner–Mindlin model, the existence of Fortin operators remains open. Second, in cases where the stability analysis requires Poincaré-type estimates, norms in test spaces have to be properly scaled in order for DPG schemes to be robust for larger domains. Otherwise approximations suffer from long pre-asymptotic ranges of reduced convergence, a type of locking phenomenon. For a detailed analysis

we refer to [27], and we note that a scaling of norms is required for least-squares methods as well, see [15, Section 3]. In order to not complicate the presentation, we restrain from providing all the details that are required to have a domain-robust approximation. Instead, we collect all the needed changes in §4.3 and state the corresponding error estimates without proof.

An overview of the remainder is as follows. In the next section we specify the model problem, prescribe allowed boundary conditions, define some basic spaces, and present the Helmholtz decomposition. Section 3.1 gives all the definitions and technical results on spaces, norms, and trace operators. In Section 4 we make use of the trace operators and spaces to derive our ultra-weak formulation. We list the three variational stages and claim their stability in Theorem 5 and Corollary 6. Subsequently we present a discretization of the three stages and state their  $t$ -robust quasi-optimal convergence in Theorem 7. In the remainder of Section 4 we provide proofs of the stated results. In order to prove that our scheme is locking free, certain regularity results are needed. They usually require convexity of the domain and hard-clamped boundary conditions. In Section 5 we specify these assumptions, and recall from [3] that they are satisfied for a special case. We then state and prove a locking-free a priori error estimate for a lowest-order scheme that uses canonical bases. Finally, in Section 6 we present several numerical experiments that illustrate our theoretical results. In particular, they confirm that our scheme is locking free for convex hard-clamped plates. It exhibits locking-free approximations also for other boundary conditions and an example on a non-convex polygonal plate.

Throughout the paper, notation  $a \lesssim b$  means that  $a \leq cb$  with an unspecified generic constant  $c > 0$  that is independent of the (scaled) plate thickness  $t$  and the underlying mesh  $\mathcal{T}$ . Notation  $a \gtrsim b$  means that  $b \lesssim a$ , and  $a \simeq b$  indicates  $a \lesssim b$  and  $a \gtrsim b$ .

## 2 Model problem

Let  $\Omega \subset \mathbb{R}^2$  be a bounded simply connected Lipschitz domain with boundary  $\Gamma = \partial\Omega$ . More specifically, for simplicity of the discrete analysis, we assume that  $\Omega$  is a polygon. We are considering the Reissner–Mindlin plate bending model with linearly elastic, homogeneous and isotropic material, described by the constitutive relations

$$\begin{aligned} \mathbf{q} &= \kappa G t (\nabla u - \boldsymbol{\psi}), \\ \mathbf{M} &= -Dt^3 [\nu \operatorname{tr}(\boldsymbol{\varepsilon}\boldsymbol{\psi}) \mathbf{I} + (1 - \nu) \boldsymbol{\varepsilon}\boldsymbol{\psi}] \end{aligned} \tag{1}$$

and the equilibrium equations

$$\begin{aligned} -\operatorname{div} \mathbf{q} &= f, \\ \mathbf{q} &= \operatorname{div} \mathbf{M} \end{aligned}$$

on  $\Omega$ . Here,  $\Omega$  is the mid-surface of the plate with thickness  $t > 0$ ,  $f$  the transversal bending load,  $u$  the transverse deflection,  $\boldsymbol{\psi}$  the rotation vector,  $\mathbf{q}$  the shear force vector,  $\mathbf{M}$  the bending moment tensor,  $\mathbf{I}$  the identity tensor, and  $\boldsymbol{\varepsilon}$  the symmetric gradient,  $\boldsymbol{\varepsilon}\boldsymbol{\psi} := \frac{1}{2}(\nabla\boldsymbol{\psi} + (\nabla\boldsymbol{\psi})^\top)$ .

Furthermore,  $\nu \in (-1, 1/2]$  is the Poisson ratio,  $\kappa > 0$  the shear correction factor, and

$$G = \frac{E}{2(1+\nu)}, \quad D = \frac{E}{12(1-\nu^2)}$$

with the Young modulus  $E > 0$ . The operator  $\operatorname{div}$  is the standard divergence, and  $\mathbf{div}$  is the row-wise divergence when writing second-order tensors as  $2 \times 2$  matrix functions.

Relation (1) between  $\mathbf{M}$  and  $\boldsymbol{\psi}$  can be written like

$$\mathbf{M} = -t^3 \mathcal{C} \boldsymbol{\varepsilon} \boldsymbol{\psi}$$

where  $\mathcal{C}$  is the positive definite plane stress constitutive tensor that is independent of  $t$ . It is an isomorphism within the space  $\mathbb{L}_2^s(\Omega)$  of symmetric  $L_2(\Omega)$ -tensors. Since the dependence of the problem on  $\kappa G$  is not critical, we simply select  $\kappa G = 1$ . Then, re-scaling  $f \rightarrow t^3 f$ ,  $\mathbf{M} \rightarrow t^3 \mathbf{M}$  and  $\mathbf{q} \rightarrow t^3 \mathbf{q}$ , the Reissner–Mindlin model simplifies to the system

$$-\operatorname{div} \mathbf{q} = f, \quad \mathbf{M} + \mathcal{C} \boldsymbol{\varepsilon} \boldsymbol{\psi} = 0, \quad \mathbf{div} \mathbf{M} - \mathbf{q} = 0, \quad \mathbf{q} = t^{-2}(\nabla u - \boldsymbol{\psi}). \quad (2)$$

Canonical (homogeneous) boundary conditions are given on mutually exclusive subsets  $\Gamma_{\text{hc}}$ ,  $\Gamma_{\text{sc}}$ ,  $\Gamma_{\text{hss}}$ ,  $\Gamma_{\text{sss}}$ ,  $\Gamma_{\text{f}}$  of  $\Gamma$  (for simplicity we assume that they are connected; they can be empty and the closure of their union equals  $\Gamma$ ),

$$\begin{aligned} \text{hard clamped (hc):} & \quad \boldsymbol{\psi} = 0, \quad u = 0 & \quad \text{on } \Gamma_{\text{hc}}, \\ \text{soft clamped (sc):} & \quad \boldsymbol{\psi} \cdot \mathbf{n} = \mathbf{t} \cdot \mathbf{M} \mathbf{n} = u = 0 & \quad \text{on } \Gamma_{\text{sc}}, \\ \text{hard simple support (hss):} & \quad \mathbf{n} \cdot \mathbf{M} \mathbf{n} = \boldsymbol{\psi} \cdot \mathbf{t} = u = 0 & \quad \text{on } \Gamma_{\text{hss}}, \\ \text{soft simple support (sss):} & \quad \mathbf{M} \mathbf{n} = 0, \quad u = 0 & \quad \text{on } \Gamma_{\text{sss}}, \\ \text{free (f):} & \quad \mathbf{M} \mathbf{n} = 0, \quad \mathbf{q} \cdot \mathbf{n} = 0 & \quad \text{on } \Gamma_{\text{f}}. \end{aligned}$$

Here,  $\mathbf{n}$  and  $\mathbf{t}$  are the unit exterior normal and tangential vectors along  $\Gamma$ , respectively.

In the following we use the notation  $\Gamma_{\text{u}} := \Gamma \setminus \bar{\Gamma}_{\text{f}}$  for the part of the boundary with imposed zero deflection. Throughout, our assumptions are that  $\Gamma_{\text{u}}$  has positive measure and that the boundary condition for rotation  $\boldsymbol{\psi}$  (referred to as “ $\text{bc}(\boldsymbol{\psi})$ ”) eliminates “rigid rotations” so that the Korn inequality  $\|\boldsymbol{\psi}\| \lesssim \|\boldsymbol{\varepsilon} \boldsymbol{\psi}\|$  holds. Here,  $\|\cdot\|$  denotes the  $L_2(\Omega)$ -norm, generically for scalar, vector and tensor-valued functions. In the case of  $\Gamma_{\text{f}} = \emptyset$  we will need the quotient space  $L_2(\Omega)/\mathbb{R}$  with quotient norm. Also, some scaling will be different for different boundary conditions. For brevity we will write

$$\begin{aligned} \text{if } \Gamma_{\text{f}} = \emptyset : & \quad L_2^*(\Omega) := L_2(\Omega)/\mathbb{R}, \quad H_*^1(\Omega) := H^1(\Omega)/\mathbb{R}, \quad \|\cdot\|_* := \inf_{c \in \mathbb{R}} \|\cdot - c\|, \\ \text{if } \Gamma_{\text{f}} \neq \emptyset : & \quad L_2^*(\Omega) := L_2(\Omega), \quad H_*^1(\Omega) := H^1(\Omega), \quad \|\cdot\|_* := \|\cdot\|, \\ \text{if } \Gamma_{\text{sc}} = \Gamma_{\text{sss}} = \emptyset : & \quad t_* := 1, \\ \text{if } \Gamma_{\text{sc}} \cup \Gamma_{\text{sss}} \neq \emptyset : & \quad t_* := t. \end{aligned} \quad (3)$$

Here,  $H^1(\Omega)$  is the standard Sobolev space. We note that parameter  $t_*$  will appear as a weighting factor in the test norm and determines the weighting  $t_*^{-1}$  of one of the unknown trace terms.

Now, in case of boundary conditions implying  $\Gamma_{\text{sc}} = \Gamma_{\text{sss}} = \emptyset$ , assignment  $t_* = 1$  implies that weight  $t_*^{-1}$  on the ansatz side does not blow up when  $t \rightarrow 0$ . This will be important when proving that our scheme is locking free. Whether the selection of  $t_* = 1$  is possible will become clear in the stability analysis of the adjoint problem, cf. §4.1 below.

In order to formulate the needed Korn and Poincaré inequalities we introduce some spaces with boundary conditions. We denote  $\mathbf{H}^1(\Omega) := (H^1(\Omega))^2$  and define

$$\mathbf{H}_\psi^1(\Omega) := \{\boldsymbol{\chi} \in \mathbf{H}^1(\Omega); \boldsymbol{\chi} \text{ satisfies bc}(\psi)\}, \quad (4a)$$

$$H_u^1(\Omega) := \{v \in H^1(\Omega); v = 0 \text{ on } \Gamma \setminus \bar{\Gamma}_f\}, \quad (4b)$$

$$H_p^1(\Omega) := \{v \in H_*^1(\Omega); v|_{\Gamma_f} = 0\}. \quad (4c)$$

Notation  $H_p^1(\Omega)$  stems from a variable  $p$ , later introduced through a Helmholtz decomposition, with boundary condition complementary to that of  $u$ . Then we will use the Korn and Poincaré inequalities

$$\|\boldsymbol{\chi}\| + \|\nabla \boldsymbol{\chi}\| \lesssim \|\boldsymbol{\epsilon} \boldsymbol{\chi}\| \quad \forall \boldsymbol{\chi} \in \mathbf{H}_\psi^1(\Omega), \quad (5)$$

$$\|v\|_* \lesssim \|\nabla v\| \quad \forall v \in H_p^1(\Omega). \quad (6)$$

**Remark 1.** *Inequalities (5), (6) are valid for a fixed domain. The hidden constants depend on the size of  $\Omega$ . Since these bounds influence the selection of test norms for our DPG scheme, it is critical to include scaling parameters when considering larger, even moderately sized, domains. We refer to [27] for a detailed discussion. For ease of presentation, our analysis does not consider such a scaling, i.e., we assume  $\text{diam}(\Omega)$  to be the length unit. In Section 4.3, we specify the changes that are required in order to have a DPG scheme that is robust with respect to the diameter of  $\Omega$ .*

## 2.1 Helmholtz decomposition

Let us introduce the operators

$$\mathbf{curl} z := (\partial_y z, -\partial_x z)^T, \quad \text{rot } \mathbf{q} := \partial_x q_y - \partial_y q_x \quad \text{for } \mathbf{q} = (q_x, q_y)^T \quad (\text{formal adjoints}).$$

Following [13, 3], we use a Helmholtz decomposition of  $\mathbf{q} = t^{-2}(\nabla u - \boldsymbol{\psi})$ . Defining

$$r \in H_u^1(\Omega) : \quad (\nabla r, \nabla \delta r) = (f, \delta r) \quad \forall \delta r \in H_u^1(\Omega) \quad (7)$$

(with  $L_2(\Omega)$ -duality  $(\cdot, \cdot)$ ) it follows that  $\text{div}(\mathbf{q} - \nabla r) = 0$  so that

$$\mathbf{q} = t^{-2}(\nabla u - \boldsymbol{\psi}) = \nabla r + \mathbf{curl} p \quad (8)$$

with  $p \in H^1(\Omega)$  satisfying

$$\text{rot}(t^2 \mathbf{curl} p + \boldsymbol{\psi}) = 0 \quad \text{in } \Omega. \quad (9)$$

By definition (7) of  $r$  we have that  $r = 0$  on  $\Gamma_u$  and  $\mathbf{n} \cdot \nabla r = 0$  on  $\Gamma_f$ . Therefore, since  $\mathbf{q} \cdot \mathbf{n} = 0$  on  $\Gamma_f$  and  $\mathbf{q} - \nabla r = \mathbf{curl} p$ , it follows that  $\mathbf{n} \cdot \mathbf{curl} p = 0$  on  $\Gamma_f$ ,  $p|_{\Gamma_f}$  is constant (we select 0). Furthermore, since  $\mathbf{t} \cdot \nabla r = \mathbf{t} \cdot \nabla u = 0$  on  $\Gamma_u$  and  $\nabla u - t^2 \nabla r = t^2 \mathbf{curl} p + \boldsymbol{\psi}$ , we obtain the following boundary conditions for  $p$ :

$$p = 0 \quad \text{on} \quad \Gamma_f, \quad \mathbf{t} \cdot (t^2 \mathbf{curl} p + \boldsymbol{\psi}) = 0 \quad \text{on} \quad \Gamma_u.$$

Now, introducing  $\boldsymbol{\eta} := t \mathbf{curl} p$ , substituting  $\mathbf{q}$  by decomposition (8), system (2) becomes

$$\mathbf{div} \mathbf{M} - \mathbf{curl} p = \nabla r, \tag{10a}$$

$$\mathbf{M} + \mathcal{C}\varepsilon \boldsymbol{\psi} = 0, \tag{10b}$$

$$\text{rot}(t\boldsymbol{\eta} + \boldsymbol{\psi}) = 0, \tag{10c}$$

$$t \mathbf{curl} p - \boldsymbol{\eta} = 0 \tag{10d}$$

in  $\Omega$ , and  $u$  is determined by

$$u \in H_u^1(\Omega) : \quad (\nabla u, \nabla \delta u) = t^2 (f, \delta u) + (\boldsymbol{\psi}, \nabla \delta u) \quad \forall \delta u \in H_u^1(\Omega). \tag{11}$$

In the following we derive an ultraweak formulation for problem (10), considering different boundary conditions.

### 3 Spaces and trace operators

In the following let  $\mathcal{T} = \{T\}$  denote a mesh of pairwise disjoint Lipschitz elements  $T$  covering  $\Omega$ ,  $\bar{\Omega} = \cup_{T \in \mathcal{T}} \bar{T}$ . For a Lipschitz domain  $\omega \subset \Omega$  we use the Lebesgue spaces of scalar, vector and  $2 \times 2$  tensor fields  $L_2(\omega)$ ,  $\mathbf{L}_2(\omega)$  and  $\mathbb{L}_2(\omega)$ , with generic norm  $\|\cdot\|_\omega$ , denote by  $\mathbb{L}_2^s(\omega)$  the space of symmetric tensors, and define the Sobolev spaces

$$\mathbf{H}(\text{rot}, \omega) := \{\boldsymbol{\rho} \in \mathbf{L}_2(\omega); \text{rot} \boldsymbol{\rho} \in L_2(\omega)\},$$

$$\mathbf{H}(\mathbf{div}, \omega) := \{\mathbf{S} \in \mathbb{L}_2(\omega); \mathbf{div} \mathbf{S} \in L_2(\omega)\}, \quad \mathbf{H}^s(\mathbf{div}, \omega) := \mathbf{H}(\mathbf{div}, \omega) \cap \mathbb{L}_2^s(\omega).$$

Corresponding product spaces with respect to  $\mathcal{T}$  are denoted analogously, replacing  $\omega$  with  $\mathcal{T}$ . For instance,  $\mathbf{H}(\text{rot}, \mathcal{T}) := \prod_{T \in \mathcal{T}} \mathbf{H}(\text{rot}, T)$  with product norm

$$\left( \|\boldsymbol{\rho}\|^2 + \|\text{rot} \boldsymbol{\rho}\|_{\mathcal{T}}^2 \right)^{1/2} \quad \text{where} \quad \|\text{rot} \boldsymbol{\rho}\|_{\mathcal{T}}^2 := \sum_{T \in \mathcal{T}} \|\text{rot} \boldsymbol{\rho}\|_T^2 \quad (\boldsymbol{\rho} \in \mathbf{H}(\text{rot}, \mathcal{T})).$$

Furthermore, we need the spaces

$$V_1(\mathcal{T}) := \mathbf{H}^1(\mathcal{T}) \times \mathbf{H}(\text{rot}, \mathcal{T}), \tag{12a}$$

$$V_2(\mathcal{T}) := \mathbf{H}(\mathbf{div}, \mathcal{T}) \times H_*^1(\mathcal{T}), \quad V_2^s(\mathcal{T}) := \mathbf{H}^s(\mathbf{div}, \mathcal{T}) \times H_*^1(\mathcal{T}), \tag{12b}$$

$$V(\mathcal{T}) := V_1(\mathcal{T}) \times V_2^s(\mathcal{T}). \tag{12c}$$

with  $H_*^1(\mathcal{T}) := H^1(\mathcal{T})/\mathbb{R}$  when  $\Gamma_f = \emptyset$  and  $H_*^1(\mathcal{T}) := H^1(\mathcal{T})$  otherwise, and norms

$$\begin{aligned}\|(\boldsymbol{\chi}, \boldsymbol{\rho})\|_{V_1(\mathcal{T}, t)}^2 &:= \|\boldsymbol{\chi}\|^2 + \|\nabla \boldsymbol{\chi}\|_{\mathcal{T}}^2 + \|\boldsymbol{\rho}\|^2 + t^{-2} \|\operatorname{rot}(t\boldsymbol{\rho} + \boldsymbol{\chi})\|_{\mathcal{T}}^2, \\ \|(\boldsymbol{S}, v)\|_{V_2(\mathcal{T}, t)}^2 &:= \|\boldsymbol{S}\|^2 + t_*^2 \|v\|_*^2 + \|\operatorname{div} \boldsymbol{S} - \operatorname{curl} v\|_{\mathcal{T}}^2 + t^2 \|\operatorname{curl} v\|_{\mathcal{T}}^2, \\ \|(\boldsymbol{\chi}, \boldsymbol{\rho}, \boldsymbol{S}, v)\|_{V(\mathcal{T}, t)}^2 &:= \|(\boldsymbol{\chi}, \boldsymbol{\rho})\|_{V_1(\mathcal{T}, t)}^2 + \|(\boldsymbol{S}, v)\|_{V_2(\mathcal{T}, t)}^2\end{aligned}$$

for  $(\boldsymbol{\chi}, \boldsymbol{\rho}) \in V_1(\mathcal{T})$  and  $(\boldsymbol{S}, v) \in V_2(\mathcal{T})$ . For notation  $t_*$  and  $\|\cdot\|_*$ , recall definition (3).

In our variational setting,  $V(\mathcal{T}) = V_1(\mathcal{T}) \times V_2^s(\mathcal{T})$  will be the test space with symmetric tensors  $\boldsymbol{S} \in \boldsymbol{H}^s(\operatorname{div}, \mathcal{T})$  whereas the larger space  $V_2(\mathcal{T})$  will be needed to define traces of  $\boldsymbol{M} \in \boldsymbol{H}(\operatorname{div}, \Omega)$  without symmetry condition. Specifically, our trace variables will come from the trial spaces

$$U_1 := \boldsymbol{H}^1(\Omega) \times \boldsymbol{H}(\operatorname{rot}, \Omega) \subset V_1(\mathcal{T}), \quad U_2 := \boldsymbol{H}(\operatorname{div}, \Omega) \times H_*^1(\Omega) \subset V_2(\mathcal{T}) \quad (13)$$

with norms

$$\begin{aligned}\|(\boldsymbol{\psi}, \boldsymbol{\eta})\|_{U_1(t)}^2 &:= \|\boldsymbol{\psi}\|^2 + \|\boldsymbol{\varepsilon} \boldsymbol{\psi}\|^2 + \|\boldsymbol{\eta}\|^2 + t_*^{-2} \|\operatorname{rot}(t\boldsymbol{\eta} + \boldsymbol{\psi})\|^2, \\ \|(\boldsymbol{M}, p)\|_{U_2(t)}^2 &:= \|\boldsymbol{M}\|^2 + t^2 \|p\|_*^2 + \|\operatorname{div} \boldsymbol{M} - \operatorname{curl} p\|^2 + t^2 \|\operatorname{curl} p\|^2\end{aligned}$$

for  $(\boldsymbol{\psi}, \boldsymbol{\eta}) \in U_1$  and  $(\boldsymbol{M}, p) \in U_2$ . Note the subtle difference in the norms  $\|\nabla \boldsymbol{\chi}\|_{\mathcal{T}}$  with full gradient on the test side and  $\|\boldsymbol{\varepsilon} \boldsymbol{\psi}\|$  with symmetric part of the gradient on the trial side. Of course,

$$\|(\boldsymbol{\psi}, \boldsymbol{\eta})\|_{U_1(t)}^2 \simeq \|\boldsymbol{\psi}\|^2 + \|\nabla \boldsymbol{\psi}\|^2 + \|\boldsymbol{\eta}\|^2 + t^2 \|\operatorname{rot} \boldsymbol{\eta}\|^2 \quad \text{if } t_* = 1$$

uniformly in  $t > 0$ . In (13) we have identified functions of  $\mathcal{T}$ -product spaces with their counterparts on  $\Omega$  defined in the piecewise sense, and will continue to do so. Taking the boundary conditions into account (recall definition (4)) the spaces become

$$U_{1,0}(t) := \{(\boldsymbol{\psi}, \boldsymbol{\eta}) \in \boldsymbol{H}_\psi^1(\Omega) \times \boldsymbol{H}(\operatorname{rot}, \Omega); \boldsymbol{t} \cdot (t\boldsymbol{\eta} + \boldsymbol{\psi})|_{\Gamma_u} = 0\}, \quad (14a)$$

$$U_{2,0}(t) := \{(\boldsymbol{M}, p) \in \boldsymbol{H}(\operatorname{div}, \Omega) \times H_p^1(\Omega); \boldsymbol{t} \cdot \boldsymbol{M} \boldsymbol{n}|_{\Gamma_{sc}} = \boldsymbol{n} \cdot \boldsymbol{M} \boldsymbol{n}|_{\Gamma_{hss}} = 0, \boldsymbol{M} \boldsymbol{n}|_{\Gamma_{sss} \cup \Gamma_f} = 0\}. \quad (14b)$$

### 3.1 Traces

We define trace operators

$$\operatorname{tr}^\psi : V_1(\mathcal{T}) \rightarrow V_2^s(\mathcal{T})', \quad \operatorname{tr}^M : V_2(\mathcal{T}) \rightarrow V_1(\mathcal{T})'$$

by

$$\begin{aligned}\langle \operatorname{tr}^\psi(\boldsymbol{\chi}, \boldsymbol{\rho}), (\boldsymbol{S}, v) \rangle_{\mathcal{S}} &:= \langle \boldsymbol{\chi}, \operatorname{div} \boldsymbol{S} - \operatorname{curl} v \rangle_{\mathcal{T}} - \langle \boldsymbol{\rho}, t \operatorname{curl} v \rangle_{\mathcal{T}} + \langle \nabla \boldsymbol{\chi}, \boldsymbol{S} \rangle_{\mathcal{T}} + \langle \operatorname{rot}(t\boldsymbol{\rho} + \boldsymbol{\chi}), v \rangle_{\mathcal{T}}, \\ \langle \operatorname{tr}^M(\boldsymbol{M}, p), (\boldsymbol{\chi}, \boldsymbol{\rho}) \rangle_{\mathcal{S}} &:= \langle \operatorname{tr}^\psi(\boldsymbol{\chi}, \boldsymbol{\rho}), (\boldsymbol{M}, p) \rangle_{\mathcal{S}}\end{aligned}$$

for  $(\boldsymbol{\chi}, \boldsymbol{\rho}) \in V_1(\mathcal{T})$ ,  $(\boldsymbol{S}, v) \in V_2^s(\mathcal{T})$ , and  $(\boldsymbol{M}, p) \in V_2(\mathcal{T})$ . Here,  $(\cdot, \cdot)_{\mathcal{T}}$  denotes the generic  $L_2(\mathcal{T})$ -duality for scalar, vector and tensor fields. That is, appearing differential operators are taken

piecewise on  $\mathcal{T}$ . Of course, for symmetric  $\mathbf{S}$ ,  $(\nabla\boldsymbol{\chi}, \mathbf{S})_{\mathcal{T}} = (\boldsymbol{\varepsilon}\boldsymbol{\chi}, \mathbf{S})_{\mathcal{T}}$  in the definition of operator  $\text{tr}^{\psi}$ .

Now, the restriction of  $\text{tr}^{\psi}$  and  $\text{tr}^M$  to the corresponding spaces of continuous functions gives rise to the trace spaces

$$\mathbf{H}_0^{\psi}(\mathcal{S}, t) := \text{tr}^{\psi}(U_{1,0}(t)), \quad \mathbf{H}_0^M(\mathcal{S}, t) := \text{tr}^M(U_{2,0}(t))$$

with norms

$$\|\widehat{\psi\boldsymbol{\eta}}\|_{\psi, t} := \inf\{\|(\boldsymbol{\psi}, \boldsymbol{\eta})\|_{U_1(t)}; \text{tr}^{\psi}((\boldsymbol{\psi}, \boldsymbol{\eta})) = \widehat{\psi\boldsymbol{\eta}}\} \quad (\widehat{\psi\boldsymbol{\eta}} \in \mathbf{H}_0^{\psi}(\mathcal{S}, t)), \quad (15a)$$

$$\|\widehat{M\boldsymbol{p}}\|_{M, t} := \inf\{\|(\mathbf{M}, \boldsymbol{p})\|_{U_2(t)}; \text{tr}^M((\mathbf{M}, \boldsymbol{p})) = \widehat{M\boldsymbol{p}}\} \quad (\widehat{M\boldsymbol{p}} \in \mathbf{H}_0^M(\mathcal{S}, t)). \quad (15b)$$

The following statements relate canonical trace norms with their counterparts by duality.

**Lemma 2.**

$$\|\widehat{\psi\boldsymbol{\eta}}\|_{\psi, t} = \sup_{0 \neq (\mathbf{S}, v) \in V_2^s(\mathcal{T})} \frac{\langle \widehat{\psi\boldsymbol{\eta}}, (\mathbf{S}, v) \rangle_{\mathcal{S}}}{\|(\mathbf{S}, v)\|_{V_2(\mathcal{T}, t)}} \quad (\widehat{\psi\boldsymbol{\eta}} \in \mathbf{H}_0^{\psi}(\mathcal{S}, t)),$$

$$\|\widehat{M\boldsymbol{p}}\|_{M, t} = \sup_{0 \neq (\boldsymbol{\chi}, \boldsymbol{\rho}) \in V_1(\mathcal{T})} \frac{\langle \widehat{M\boldsymbol{p}}, (\boldsymbol{\chi}, \boldsymbol{\rho}) \rangle_{\mathcal{S}}}{\|(\boldsymbol{\chi}, \boldsymbol{\rho})\|_{V_1(\mathcal{T}, t)}} \quad (\widehat{M\boldsymbol{p}} \in \mathbf{H}_0^M(\mathcal{S}, t)).$$

Here, the dualities between the trace spaces and corresponding product test spaces are defined in the canonical way, to be consistent with the definition of the trace operators.

*Proof.* These statements follow from standard arguments, see [20, Lemma A.10] for the first setting, and [30, Proof of Lemma 4] for a framework that applies to our variational formulation. In [29, Proof of Proposition 3]) this framework is recalled more briefly.  $\square$

**Remark 3.** We note that for sufficiently smooth functions  $(\boldsymbol{\psi}, \boldsymbol{\eta}), (\boldsymbol{\chi}, \boldsymbol{\rho}) \in U_1, (\mathbf{M}, \boldsymbol{p}), (\mathbf{S}, v) \in U_2$  the traces reduce to a mixture of classical traces on  $\Gamma$  of scalar functions, tangential traces of vector functions, and normal traces of tensors (with  $L_2(\Gamma)$ -bilinear form  $\langle \cdot, \cdot \rangle_{\Gamma}$ ):

$$\langle \text{tr}^{\psi}(\boldsymbol{\psi}, \boldsymbol{\eta}), (\mathbf{S}, v) \rangle_{\mathcal{S}} = \langle \boldsymbol{\psi}, \mathbf{S}\mathbf{n} + v\mathbf{t} \rangle_{\Gamma} + t \langle \boldsymbol{\eta} \cdot \mathbf{t}, v \rangle_{\Gamma} = \langle \boldsymbol{\psi}, \mathbf{S}\mathbf{n} \rangle_{\Gamma} + \langle (t\boldsymbol{\eta} + \boldsymbol{\psi}) \cdot \mathbf{t}, v \rangle_{\Gamma},$$

$$\langle \text{tr}^M(\mathbf{M}, \boldsymbol{p}), (\boldsymbol{\chi}, \boldsymbol{\rho}) \rangle_{\mathcal{S}} = \langle \mathbf{M}\mathbf{n} + \boldsymbol{p}\mathbf{t}, \boldsymbol{\chi} \rangle_{\Gamma} + t \langle \boldsymbol{p}, \boldsymbol{\rho} \cdot \mathbf{t} \rangle_{\Gamma} = \langle \mathbf{M}\mathbf{n}, \boldsymbol{\chi} \rangle_{\Gamma} + \langle \boldsymbol{p}, (t\boldsymbol{\rho} + \boldsymbol{\chi}) \cdot \mathbf{t} \rangle_{\Gamma}.$$

For general functions of the above spaces, these are dualities between Sobolev spaces of orders  $\pm 1/2$  on  $\Gamma$ . Furthermore, for test functions of product spaces,  $(\mathbf{S}, v) \in V_2^s(\mathcal{T})$  and  $(\boldsymbol{\chi}, \boldsymbol{\rho}) \in V_1(\mathcal{T})$ , traces  $\text{tr}^{\psi}(\boldsymbol{\psi}, \boldsymbol{\eta})$  and  $\text{tr}^M(\mathbf{M}, \boldsymbol{p})$  live on the skeleton  $\mathcal{S} = \{\partial T; T \in \mathcal{T}\}$ .

**Lemma 4.** Let  $(\boldsymbol{\chi}, \boldsymbol{\rho}, \mathbf{S}, v) \in V(\mathcal{T})$  and  $t > 0$  be given. The equivalences

$$\begin{aligned} (\boldsymbol{\chi}, \boldsymbol{\rho}) \in U_{1,0}(t) &\Leftrightarrow \langle \text{tr}^M(\mathbf{M}, \boldsymbol{p}), (\boldsymbol{\chi}, \boldsymbol{\rho}) \rangle_{\mathcal{S}} = 0 \quad \forall (\mathbf{M}, \boldsymbol{p}) \in U_{2,0}(t), \\ (\mathbf{S}, v) \in U_{2,0}(t) &\Leftrightarrow \langle \text{tr}^{\psi}(\boldsymbol{\psi}, \boldsymbol{\eta}), (\mathbf{S}, v) \rangle_{\mathcal{S}} = 0 \quad \forall (\boldsymbol{\psi}, \boldsymbol{\eta}) \in U_{1,0}(t) \end{aligned}$$

hold true.



*Proof.* In both cases, direction “ $\Rightarrow$ ” can be seen by following Remark 3 and observing that all the dualities on  $\Gamma$  vanish due to the boundary conditions of spaces  $U_{1,0}(t)$  and  $U_{2,0}(t)$ . To show direction “ $\Leftarrow$ ” in the first statement, let  $(\boldsymbol{\chi}, \boldsymbol{\rho}) \in V_1(\mathcal{T})$  be given with  $\langle \text{tr}^M(\mathbf{M}, p), (\boldsymbol{\chi}, \boldsymbol{\rho}) \rangle_{\mathcal{S}} = 0$  for any  $(\mathbf{M}, p) \in U_{2,0}(t)$ . First, selecting  $p = 0$ , this gives

$$0 = (\boldsymbol{\chi}, \mathbf{div} \mathbf{M}) + (\nabla \boldsymbol{\chi}, \mathbf{M})_{\mathcal{T}} \quad \forall \mathbf{M} \in \mathbf{H}(\mathbf{div}, \Omega) \quad \text{“plus boundary condition”,}$$

that is,  $\boldsymbol{\chi} \in \mathbf{H}^1(\Omega)$ . Second, selecting  $\mathbf{M} = 0$ , we conclude that

$$0 = (\boldsymbol{\chi}, -\mathbf{curl} p) - (\boldsymbol{\rho}, t \mathbf{curl} p) + (\text{rot}(t\boldsymbol{\rho} + \boldsymbol{\chi}), p)_{\mathcal{T}} \quad \forall p \in H_*^1(\Omega) \quad \text{“plus boundary condition”,}$$

that is,  $t\boldsymbol{\rho} + \boldsymbol{\chi} \in \mathbf{H}(\text{rot}, \Omega)$ . Therefore,  $(\boldsymbol{\chi}, \boldsymbol{\rho}) \in U_1$ . The boundary conditions  $(\boldsymbol{\chi}, \boldsymbol{\rho}) \in U_{1,0}(t)$  follow from the corresponding conditions in  $U_{2,0}(t)$  and the dualities observed in Remark 3.

The proof of “ $\Leftarrow$ ” in the second statement is analogous. Specifically, selecting  $(\boldsymbol{\psi}, \boldsymbol{\eta}) = (0, \boldsymbol{\eta})$  yields  $v \in H^1(\Omega)$ , and selecting  $(\boldsymbol{\psi}, \boldsymbol{\eta}) = (\boldsymbol{\psi}, 0)$  shows that  $\mathbf{S} \in \mathbf{H}(\mathbf{div}, \Omega)$ . The symmetry  $\mathbf{S} \in \mathbf{H}^s(\mathbf{div}, \Omega)$  is due to the imposed symmetry in  $V_2^s(\mathcal{T})$ , cf. (12). Therefore,  $(\mathbf{S}, v) \in U_2$ , and the boundary conditions  $(\mathbf{S}, v) \in U_{2,0}(t)$  can be seen as before.  $\square$

## 4 Three-stage variational formulation and discretization

We obtain a variational formulation of problem (10) by testing, respectively, (10a), (10b), (10c), (10d) with  $-\boldsymbol{\chi}$ ,  $\mathcal{C}^{-1}\mathbf{S}$ ,  $v$ ,  $\boldsymbol{\rho}$ , and using trace operators  $\text{tr}^\psi$ ,  $\text{tr}^M$ . This gives

$$\begin{aligned} b((\boldsymbol{\psi}, \boldsymbol{\eta}, \mathbf{M}, p, \widehat{\boldsymbol{\psi}\boldsymbol{\eta}}, \widehat{Mp}), (\boldsymbol{\chi}, \boldsymbol{\rho}, \mathbf{S}, v)) := \\ (\boldsymbol{\psi}, \mathbf{curl} v - \mathbf{div} \mathbf{S})_{\mathcal{T}} + (\mathbf{M}, \mathcal{C}^{-1}\mathbf{S} + \varepsilon \boldsymbol{\chi})_{\mathcal{T}} + (\boldsymbol{\eta}, t \mathbf{curl} v - \boldsymbol{\rho})_{\mathcal{T}} + (p, \text{rot}(t\boldsymbol{\rho} + \boldsymbol{\chi}))_{\mathcal{T}} \\ + \langle \widehat{\boldsymbol{\psi}\boldsymbol{\eta}}, (\mathbf{S}, v) \rangle_{\mathcal{S}} - \langle \widehat{Mp}, (\boldsymbol{\chi}, \boldsymbol{\rho}) \rangle_{\mathcal{S}} = -(\nabla r, \boldsymbol{\chi}) \end{aligned}$$

with  $\widehat{\boldsymbol{\psi}\boldsymbol{\eta}} = \text{tr}^\psi(\boldsymbol{\psi}, \boldsymbol{\eta})$  and  $\widehat{Mp} = \text{tr}^M(\mathbf{M}, p)$ . A solution  $\mathbf{u} = (\boldsymbol{\psi}, \boldsymbol{\eta}, \mathbf{M}, p, \widehat{\boldsymbol{\psi}\boldsymbol{\eta}}, \widehat{Mp})$  will be sought in space  $U(t)$  defined as

$$U(t) := \mathbf{L}_2(\Omega) \times \mathbf{L}_2(\Omega) \times \mathbb{L}_2^s(\Omega) \times L_2^*(\Omega) \times \mathbf{H}_0^\psi(\mathcal{S}, t) \times \mathbf{H}_0^M(\mathcal{S}, t) \quad (16)$$

with (squared) norm

$$\|(\boldsymbol{\psi}, \boldsymbol{\eta}, \mathbf{M}, p, \widehat{\boldsymbol{\psi}\boldsymbol{\eta}}, \widehat{Mp})\|_{U(t)}^2 := \|\boldsymbol{\psi}\|^2 + \|\boldsymbol{\eta}\|^2 + \|\mathbf{M}\|^2 + t^2 \|p\|_*^2 + \|\widehat{\boldsymbol{\psi}\boldsymbol{\eta}}\|_{\psi, t}^2 + \|\widehat{Mp}\|_{M, t}^2.$$

Finally, our three-stage variational formulation of the scaled Reissner–Mindlin problem (2) consists in solving (7), then the ultraweak formulation of (10), and afterwards problem (11), that is,

$$r \in H_u^1(\Omega) : \quad (\nabla r, \nabla \delta r) = (f, \delta r) \quad \forall \delta r \in H_u^1(\Omega), \quad (17a)$$

$$\mathbf{u} = (\boldsymbol{\psi}, \boldsymbol{\eta}, \mathbf{M}, p, \widehat{\boldsymbol{\psi}\boldsymbol{\eta}}, \widehat{Mp}) \in U(t) : \quad b(\mathbf{u}, \mathbf{v}) = -(\nabla r, \boldsymbol{\chi}) \quad \forall \mathbf{v} = (\boldsymbol{\chi}, \boldsymbol{\rho}, \mathbf{S}, v) \in V(\mathcal{T}), \quad (17b)$$

$$u \in H_u^1(\Omega) : \quad (\nabla u, \nabla \delta u) = t^2(f, \delta u) + (\boldsymbol{\psi}, \nabla \delta u) \quad \forall \delta u \in H_u^1(\Omega). \quad (17c)$$

Problems (17a), (17c) are obviously well posed and we are left with proving the well-posedness of (17b).

**Theorem 5.** For given  $t \in (0, 1]$  and  $r \in H_u^1(\Omega)$ , there is a unique solution  $\mathbf{u} = (\boldsymbol{\psi}, \boldsymbol{\eta}, \mathbf{M}, p, \widehat{\boldsymbol{\psi}\eta}, \widehat{\mathbf{M}p}) \in U(t)$  to (17b). It is uniformly bounded:

$$\|\mathbf{u}\|_{U(t)} \lesssim \|\nabla r\|$$

with a hidden constant that is independent of  $r$ ,  $\mathcal{T}$ , and  $t \in (0, 1]$ . Furthermore,  $(\boldsymbol{\psi}, \boldsymbol{\eta}, \mathbf{M}, p) \in U_{1,0}(t) \times U_{2,0}(t)$  solves (10), and  $\widehat{\boldsymbol{\psi}\eta} = \text{tr}^\psi(\boldsymbol{\psi}, \boldsymbol{\eta})$ ,  $\widehat{\mathbf{M}p} = \text{tr}^M(\mathbf{M}, p)$ .

A proof of this theorem is given in §4.2. Theorem 5 immediately gives the well-posedness of (17).

**Corollary 6.** For given  $t \in (0, 1]$  and  $f \in L_2(\Omega)$ , there is a unique solution  $(r, \mathbf{u}, u) \in H_u^1(\Omega) \times U(t) \times H_u^1(\Omega)$  to (17). It is uniformly bounded:

$$\|\nabla r\|^2 + \|\mathbf{u}\|_{U(t)}^2 + \|\nabla u\|^2 \lesssim \|f\|^2$$

with a hidden constant that is independent of  $f$ ,  $\mathcal{T}$ , and  $t \in (0, 1]$ .

In order to discretize the three-stage formulation we use standard finite elements for problems (17a) and (17c), and a Petrov–Galerkin discretization of (17b) with optimal test functions, the DPG method. For simplicity we use the same mesh  $\mathcal{T}$  for the three stages and consider lowest-order approximations. Therefore, we now assume that  $\mathcal{T}$  is a regular triangular mesh. In the following,  $P^k(\mathcal{T})$  denotes the space of piecewise polynomials of degree  $k \geq 0$ . Below, we will also use the corresponding vector and tensor-valued spaces  $P^k(\mathcal{T})^2$  and  $P^k(\mathcal{T})^{2 \times 2}$ , respectively. For Poisson problems (17a), (17c) we use finite element space  $P_u^{1,c}(\mathcal{T}) := P^1(\mathcal{T}) \cap H_u^1(\Omega)$  consisting of continuous, piecewise linear polynomials. Then, selecting an approximation space  $U_h(t) \subset U(t)$  (also of lowest order), a discrete formulation of (17) is

$$r_h \in P_u^{1,c}(\mathcal{T}) : \quad (\nabla r_h, \nabla \delta r) = (f, \delta r) \quad \forall \delta r \in P_u^{1,c}(\mathcal{T}), \quad (18a)$$

$$\mathbf{u}_h = (\boldsymbol{\psi}_h, \boldsymbol{\eta}_h, \mathbf{M}_h, p_h, \widehat{\boldsymbol{\psi}\eta}_h, \widehat{\mathbf{M}p}_h) \in U_h(t) : \quad b(\mathbf{u}_h, \mathfrak{T}\delta \mathbf{u}) = -(\nabla r_h, \mathfrak{T}^\chi \delta \mathbf{u}) \quad \forall \delta \mathbf{u} \in U_h(t), \quad (18b)$$

$$u_h \in P_u^{1,c}(\mathcal{T}) : \quad (\nabla u_h, \nabla \delta u) = t^2(f, \delta u) + (\boldsymbol{\psi}_h, \nabla \delta u) \quad \forall \delta u \in P_u^{1,c}(\mathcal{T}). \quad (18c)$$

Here,  $\mathfrak{T} : U(t) \rightarrow V(\mathcal{T})$  denotes the *trial-to-test operator* defined by

$$\langle\langle \mathfrak{T}(\mathbf{u}), \mathbf{v} \rangle\rangle_{V(\mathcal{T},t)} = b(\mathbf{u}, \mathbf{v}) \quad \forall \mathbf{v} \in V(\mathcal{T}) \quad (19)$$

with inner product  $\langle\langle \cdot, \cdot \rangle\rangle_{V(\mathcal{T},t)}$  in  $V(\mathcal{T})$  that induces norm  $\|\cdot\|_{V(\mathcal{T},t)}$  and  $\mathfrak{T}^\chi \mathbf{u} := \boldsymbol{\chi}$  for  $\mathfrak{T}\mathbf{u} = (\boldsymbol{\chi}, \boldsymbol{\rho}, \mathbf{S}, v)$ .

The following theorem states the robust quasi-optimal best approximation of scheme (18).

**Theorem 7.** For given  $t \in (0, 1]$  and  $f \in L_2(\Omega)$ , there is a unique solution  $(r_h, \mathbf{u}_h, u_h)$  to (18). It satisfies

$$\|\nabla(r - r_h)\| + \|\mathbf{u} - \mathbf{u}_h\|_{U(t)} \lesssim \|\nabla(r - \tilde{r}_h)\| + \|\mathbf{u} - \tilde{\mathbf{u}}_h\|_{U(t)} \quad (20)$$

and

$$\|\nabla(u - u_h)\| \lesssim \|\nabla(r - \tilde{r}_h)\| + \|\mathbf{u} - \tilde{\mathbf{u}}_h\|_{U(t)} + \|\nabla(u - \tilde{u}_h)\| \quad (21)$$

for any  $(\tilde{r}_h, \tilde{\mathbf{u}}_h, \tilde{u}_h) \in P_u^{1,c}(\mathcal{T}) \times U_h(t) \times P_u^{1,c}(\mathcal{T})$ . Here,  $(r, \mathbf{u}, u)$  is the solution of (17), and the hidden constant is independent of  $\mathcal{T}$ ,  $t \in (0, 1]$ , the discrete spaces and datum  $f$ .

In §4.2 we give a proof of this theorem. Main ingredient is the stability of the adjoint problem of (10), which is of the same type. This is the subject of the following subsection.

**Remark 8.** (i) In practice, optimal test functions  $\mathfrak{T}\delta\mathbf{u}$  in (18b) have to be approximated. This is done by solving (19) in a finite-dimensional subspace of  $V(\mathcal{T})$ . In order to prove the well-posedness and quasi-optimal convergence of the then fully discrete scheme one has to show the existence of a corresponding Fortin operator, cf. [31].

(ii) Recall that, in the case of boundary conditions without free part ( $\Gamma_f = \emptyset$ ), both trial space  $U(t)$  and test space  $V(\mathcal{T})$  have a quotient space component. In the case of  $U(t)$ ,  $p \in L_2(\Omega)/\mathbb{R}$  is unique only up to an additive constant, cf. (16). In practice, this can be fixed by adding a rank-one term to the linear system to require  $(p, 1) = 0$ . In the case of the test space, component  $v$  of  $\mathbf{v} = (\boldsymbol{\chi}, \boldsymbol{\rho}, \mathbf{S}, v) \in V(\mathcal{T})$  is taken in  $H^1(\mathcal{T})/\mathbb{R}$ , cf. (12). This can be implemented by simply using (a discrete subspace of)  $H^1(\mathcal{T})$  instead of the quotient space since  $b(\mathbf{u}, (0, 0, 0, 1)) = 0$  for any  $\mathbf{u} \in U(t)$ .

#### 4.1 Stability of the adjoint problem

In the following we denote  $L_2^0(\Omega) := \{v \in L_2(\Omega); (v, 1) = 0\}$ .

The continuous adjoint problem is as follows. For given  $\mathbf{g}_1 \in \mathbf{L}_2(\Omega)$ ,  $\mathbf{G}_2 \in \mathbb{L}_2^s(\Omega)$ ,  $g_3 \in L_2^0(\Omega)$  if  $\Gamma_f = \emptyset$ ,  $g_3 \in L_2(\Omega)$  if  $\Gamma_f \neq \emptyset$ , and  $\mathbf{g}_4 \in \mathbf{L}_2(\Omega)$  find  $(\boldsymbol{\chi}, \boldsymbol{\rho}) \in U_{1,0}(t)$  and  $(\mathbf{S}, v) \in U_{2,0}(t)$  with  $\mathbf{S} \in \mathbb{L}_2^s(\Omega)$  such that

$$-\operatorname{div} \mathbf{S} + \operatorname{curl} v = \mathbf{g}_1, \quad (22a)$$

$$\mathcal{C}^{-1} \mathbf{S} + \varepsilon \boldsymbol{\chi} = \mathbf{G}_2, \quad (22b)$$

$$\operatorname{rot}(t\boldsymbol{\rho} + \boldsymbol{\chi}) = g_3, \quad (22c)$$

$$t \operatorname{curl} v - \boldsymbol{\rho} = \mathbf{g}_4. \quad (22d)$$

**Proposition 9.** Problem (22) has a unique solution  $(\boldsymbol{\chi}, \boldsymbol{\rho}) \in U_{1,0}(t) \subset V_1(\mathcal{T})$ ,  $(\mathbf{S}, v) \in U_{2,0}(t) \subset V_2(\mathcal{T})$  with  $\mathbf{S} \in \mathbb{L}_2^s(\Omega)$ . It is bounded as

$$\|(\boldsymbol{\chi}, \boldsymbol{\rho}, \mathbf{S}, v)\|_{V(\mathcal{T}, t)}^2 \lesssim \|\mathbf{g}_1\|^2 + \|\mathbf{G}_2\|^2 + t^{-2}\|g_3\|^2 + \|\mathbf{g}_4\|^2$$

with a generic constant that is independent of  $t > 0$ ,  $\mathcal{T}$ , and the given data  $\mathbf{g}_1, \mathbf{G}_2, g_3, \mathbf{g}_4$ .

*Proof.* We represent  $\mathbf{S}$  and  $\boldsymbol{\rho}$  via (22b) and (22d),

$$\mathbf{S} = \mathcal{C}(\mathbf{G}_2 - \varepsilon \boldsymbol{\chi}), \quad \boldsymbol{\rho} = t \operatorname{curl} v - \mathbf{g}_4. \quad (23)$$

Then, substituting  $\mathbf{S}$  in (22a) and testing with  $-\delta\boldsymbol{\chi}$ , and substituting  $\boldsymbol{\rho}$  in (22c) and testing with  $\delta v$ , we obtain the following variational problem. Find  $(\boldsymbol{\chi}, v) \in \mathbf{H}_{\psi}^1(\Omega) \times H_p^1(\Omega)$  such that

$$(\mathcal{C}\varepsilon\boldsymbol{\chi}, \varepsilon\delta\boldsymbol{\chi}) - (\operatorname{curl} v, \delta\boldsymbol{\chi}) = -(\mathbf{g}_1, \delta\boldsymbol{\chi}) + (\mathcal{C}\mathbf{G}_2, \varepsilon\delta\boldsymbol{\chi}), \quad (24a)$$

$$(\boldsymbol{\chi}, \operatorname{curl} \delta v) + t^2(\operatorname{curl} v, \operatorname{curl} \delta v) = (g_3, \delta v) + t(\mathbf{g}_4, \operatorname{curl} \delta v) \quad (24b)$$

for any  $(\boldsymbol{\delta}\boldsymbol{\chi}, \delta v) \in \mathbf{H}_\psi^1(\Omega) \times H_p^1(\Omega)$ . Here we used that

$$\begin{aligned} & (\operatorname{div} \mathbf{S}, \boldsymbol{\delta}\boldsymbol{\chi}) + (\mathbf{S}, \varepsilon \boldsymbol{\delta}\boldsymbol{\chi}) + (\operatorname{rot}(t\boldsymbol{\rho} + \boldsymbol{\chi}), \delta v) - (t\boldsymbol{\rho} + \boldsymbol{\chi}, \operatorname{curl} \delta v) \\ & = \langle \mathbf{S}\mathbf{n}, \boldsymbol{\delta}\boldsymbol{\chi} \rangle_\Gamma - \langle (t\boldsymbol{\rho} + \boldsymbol{\chi}) \cdot \mathbf{t}, \delta v \rangle_\Gamma = 0 \end{aligned}$$

due to the imposed boundary conditions, cf. (14). By coercivity of the bilinear form from (24), Korn's and Poincaré's inequalities (5), (6), there exists a unique solution to problem (24) with bound

$$\|\boldsymbol{\chi}\|^2 + \|\nabla \boldsymbol{\chi}\|^2 + t^2 \|v\|_*^2 + t^2 \|\operatorname{curl} v\|^2 \lesssim \|\mathbf{g}_1\|^2 + \|\mathbf{G}_2\|^2 + t^{-2} \|g_3\|^2 + \|\mathbf{g}_4\|^2.$$

In the case that  $\langle v, \boldsymbol{\delta}\boldsymbol{\chi} \cdot \mathbf{t} \rangle_\Gamma = 0$  for  $v \in H_p^1(\Omega)$ ,  $\boldsymbol{\delta}\boldsymbol{\chi} \in \mathbf{H}_\psi^1(\Omega)$  (that is, when  $\Gamma$  is only composed of  $\Gamma_{\text{hc}}$ ,  $\Gamma_{\text{hss}}$  and  $\Gamma_{\text{f}}$ ) then  $(\operatorname{curl} v, \boldsymbol{\delta}\boldsymbol{\chi}) = (v, \operatorname{rot} \boldsymbol{\delta}\boldsymbol{\chi})$ , and the surjectivity of

$$\operatorname{rot} : \begin{cases} \mathbf{H}_\psi^1(\Omega) \rightarrow L_2^0(\Omega) & \text{if } \Gamma_{\text{f}} = \emptyset, \\ \mathbf{H}_\psi^1(\Omega) \rightarrow L_2(\Omega) & \text{otherwise,} \end{cases}$$

(see [6, Theorem 7.1]) allows to control  $v$  more strongly due to the implied inf-sup property

$$\sup_{0 \neq \boldsymbol{\delta}\boldsymbol{\chi} \in \mathbf{H}_\psi^1(\Omega)} \frac{(\operatorname{curl} v, \boldsymbol{\delta}\boldsymbol{\chi})}{\|\varepsilon \boldsymbol{\delta}\boldsymbol{\chi}\|} \gtrsim \|v\|_*.$$

By (24a) we conclude in those cases that

$$\|v\|_*^2 \lesssim \|\varepsilon \boldsymbol{\chi}\|^2 + \|\mathbf{g}_1\|^2 + \|\mathbf{G}_2\|^2 \lesssim \|\mathbf{g}_1\|^2 + \|\mathbf{G}_2\|^2 + t^{-2} \|g_3\|^2 + \|\mathbf{g}_4\|^2.$$

Finally, the bounds for  $\|\boldsymbol{\rho}\|$ ,  $\|\mathbf{S}\|$  are implied by (23) and the previous estimates, and  $\|\operatorname{div} \mathbf{S} - \operatorname{curl} v\|_{\mathcal{T}}^2 = \|\mathbf{g}_1\|^2$ ,  $t^{-2} \|\operatorname{rot}(t\boldsymbol{\rho} + \boldsymbol{\chi})\|_{\mathcal{T}}^2 = t^{-2} \|g_3\|^2$  by (22a), (22c).  $\square$

The well-posedness of (22) implies the following injectivity.

**Corollary 10.** *Let  $t > 0$  be given. If  $\mathbf{v} \in V(\mathcal{T}, t)$  satisfies  $b(\boldsymbol{\delta}\mathbf{u}, \mathbf{v}) = 0$  for any  $\boldsymbol{\delta}\mathbf{u} \in U(t)$  then  $\mathbf{v} = 0$ .*

*Proof.* Let  $\mathbf{v} \in V(\mathcal{T}, t)$  be given with  $b(\boldsymbol{\delta}\mathbf{u}, \mathbf{v}) = 0$  for any  $\boldsymbol{\delta}\mathbf{u} \in U(t)$ . Selecting  $\boldsymbol{\delta}\mathbf{u} = (\boldsymbol{\psi}, \boldsymbol{\eta}, \mathbf{M}, p, \widehat{\boldsymbol{\psi}}\boldsymbol{\eta}, \widehat{M}p)$  with arbitrary traces  $\widehat{\boldsymbol{\psi}}\boldsymbol{\eta} \in \mathbf{H}_0^\psi(\mathcal{S}, t)$ ,  $\widehat{M}p \in \mathbf{H}_0^M(\mathcal{S}, t)$  and field variables  $\boldsymbol{\psi}, \boldsymbol{\eta}, \mathbf{M}, p$  all zero, Lemma 4 shows that  $\mathbf{v} = (\boldsymbol{\chi}, \boldsymbol{\rho}, \mathbf{S}, v) \in U_{1,0}(t) \times U_{2,0}(t)$ . We conclude that  $(\boldsymbol{\chi}, \boldsymbol{\rho}, \mathbf{S}, v)$  solves the adjoint problem (22) with homogeneous data. Therefore,  $\mathbf{v} = 0$  by Proposition 9.  $\square$

## 4.2 Proofs of Theorems 5, 7

With the preparations made, proofs of our main theorems are standard. We recall the main steps. Theorem 5 follows from the ingredients of the Babuška–Brezzi framework, verified in the following.

### 1. Boundedness of the functional.

$$-(\nabla r, \boldsymbol{\chi}) \leq \|\nabla r\| \|\boldsymbol{\chi}\| \leq \|\nabla r\| \|\mathbf{v}\|_{V(\mathcal{T}, t)} \quad \forall \mathbf{v} = (\boldsymbol{\chi}, \boldsymbol{\rho}, \mathbf{S}, v) \in V(\mathcal{T})$$

holds by definition of norm  $\|\cdot\|_{V(\mathcal{T}, t)}$ .

2. **Boundedness of the bilinear form.** We make use of Lemma 2. Then the bound  $b(\mathbf{u}, \mathbf{v}) \lesssim \|\mathbf{u}\|_{U(t)} \|\mathbf{v}\|_{V(\mathcal{T}, t)}$  for any  $\mathbf{u} \in U(t)$  and  $\mathbf{v} \in V(\mathcal{T})$  holds by the Cauchy–Schwarz inequality and the definitions of the norms.

3. **Injectivity.**

$$\sup_{0 \neq \delta \mathbf{u} \in U(t)} \frac{b(\delta \mathbf{u}, \mathbf{v})}{\|\delta \mathbf{u}\|_{U(t)}} > 0 \quad \forall \mathbf{v} \in V(\mathcal{T}, t) \setminus \{0\}$$

holds by Corollary 10.

4. **Inf-sup condition.** We follow the criteria given in [20, Theorem 3.3]: inf-sup condition

$$\sup_{0 \neq \mathbf{v} \in V(\mathcal{T})} \frac{b(\mathbf{u}; \mathbf{v})}{\|\mathbf{v}\|_{\mathfrak{B}(\mathcal{T}, t)}} \gtrsim \|\mathbf{u}\|_{U(t)} \quad \forall \mathbf{u} = (\boldsymbol{\psi}, \boldsymbol{\eta}, \mathbf{M}, p, \widehat{\boldsymbol{\psi}}\boldsymbol{\eta}, \widehat{\mathbf{M}}p) \in U(t) \quad (25)$$

follows from the inf-sup conditions

$$\sup_{0 \neq \mathbf{v} = (\boldsymbol{\chi}, \boldsymbol{\rho}, \mathbf{S}, v) \in V(\mathcal{T})} \frac{\langle \widehat{\boldsymbol{\psi}}\boldsymbol{\eta}, (\mathbf{S}, v) \rangle_{\mathcal{S}} - \langle \widehat{\mathbf{M}}p, (\boldsymbol{\chi}, \boldsymbol{\rho}) \rangle_{\mathcal{S}}}{\|\mathbf{v}\|_{V(\mathcal{T}, t)}} \gtrsim (\|\widehat{\boldsymbol{\psi}}\boldsymbol{\eta}\|_{\psi, t}^2 + \|\widehat{\mathbf{M}}p\|_{M, t}^2)^{1/2} \quad (26)$$

for any  $(\widehat{\boldsymbol{\psi}}\boldsymbol{\eta}, \widehat{\mathbf{M}}p) \in \mathbf{H}_0^\psi(\mathcal{S}, t) \times \mathbf{H}_0^M(\mathcal{S}, t)$ , and

$$\sup_{0 \neq \mathbf{v} = (\boldsymbol{\chi}, \boldsymbol{\rho}, \mathbf{S}, v) \in U_{1,0}(t) \times U_{2,0}(t)} \frac{b(\boldsymbol{\psi}, \boldsymbol{\eta}, \mathbf{M}, p, 0, 0; \mathbf{v})}{\|\mathbf{v}\|_{V(\mathcal{T}, t)}} \gtrsim (\|\boldsymbol{\psi}\|^2 + \|\boldsymbol{\eta}\|^2 + \|\mathbf{M}\|^2 + t^2\|p\|^2)^{1/2} \quad (27)$$

for any  $(\boldsymbol{\psi}, \boldsymbol{\eta}, \mathbf{M}, p) \in \mathbf{L}_2(\Omega) \times \mathbf{L}_2(\Omega) \times \mathbb{L}_2^s(\Omega) \times L_2(\Omega)$ .

By Lemma 2, inf-sup property (26) is satisfied with constant 1. In what follows, let  $p_*$  denote the representant of  $p \in L_2^*(\Omega) = L_2(\Omega)/\mathbb{R}$  with  $(p_*, 1) = 0$  if  $\Gamma_f = \emptyset$ , and  $p_* := p$  if  $\Gamma_f \neq \emptyset$ . Inf-sup condition (27) follows by application of Proposition 9 with data  $(\mathbf{g}_1, \mathbf{G}_2, g_3, \mathbf{g}_4) := (\boldsymbol{\psi}, \mathbf{M}, t^2 p_*, \boldsymbol{\eta})$  in problem (22) with solution denoted as  $\mathbf{v}^* \in U_{1,0}(t) \times U_{2,0}(t)$ :

$$\begin{aligned} \sup_{0 \neq \mathbf{v} \in U_{1,0}(t) \times U_{2,0}(t)} \frac{b(\boldsymbol{\psi}, \boldsymbol{\eta}, \mathbf{M}, p, 0, 0; \mathbf{v})}{\|\mathbf{v}\|_{V(\mathcal{T}, t)}} &\geq \frac{(\boldsymbol{\psi}, \mathbf{g}_1) + (\mathbf{M}, \mathbf{G}_2) + (p, g_3) + (\boldsymbol{\eta}, \mathbf{g}_4)}{\|\mathbf{v}^*\|_{V(\mathcal{T}, t)}} \\ &\gtrsim \frac{\|\boldsymbol{\psi}\|^2 + \|\mathbf{M}\|^2 + t^2\|p_*\|^2 + \|\boldsymbol{\eta}\|^2}{\|\mathbf{g}_1\|^2 + \|\mathbf{G}_2\|^2 + t^{-2}\|g_3\|^2 + \|\mathbf{g}_4\|^2}^{1/2} = (\|\boldsymbol{\psi}\|^2 + \|\mathbf{M}\|^2 + t^2\|p_*\|^2 + \|\boldsymbol{\eta}\|^2)^{1/2}. \end{aligned}$$

It is clear that  $(\boldsymbol{\psi}, \boldsymbol{\eta}, \mathbf{M}, p) \in U_{1,0}(t) \times U_{2,0}(t)$  solves problem (10), and that  $\widehat{\boldsymbol{\psi}}\boldsymbol{\eta} = \text{tr}^\psi(\boldsymbol{\psi}, \boldsymbol{\eta})$ ,  $\widehat{\mathbf{M}}p = \text{tr}^M(\mathbf{M}, p)$ . Therefore, Theorem 5 is proved.

It remains to prove Theorem 7. Let  $\mathbf{u}^h = (\boldsymbol{\psi}^h, \boldsymbol{\eta}^h, \mathbf{M}^h, p^h, \widehat{\boldsymbol{\psi}}\boldsymbol{\eta}^h, \widehat{\mathbf{M}}p^h)$  denote the solution of (17b) with datum  $r_h$  instead of  $r$ . We denote as  $B : U(t) \rightarrow V(\mathcal{T})'$  the operator induced by bilinear form  $b(\cdot, \cdot)$ . Interpretation of the DPG scheme as a minimum residual method and

uniform equivalence of the norms  $\|B \cdot\|_{V(\mathcal{T},t)}$  and  $\|\cdot\|_{U(t)}$  (due to the uniform boundedness of  $b(\cdot, \cdot)$  and inf-sup property (25)) show that

$$\|\mathbf{u}^h - \mathbf{u}_h\|_{U(t)} \lesssim \|\mathbf{u}^h - \tilde{\mathbf{u}}_h\|_{U(t)} \quad \forall \tilde{\mathbf{u}}_h \in U_h(t).$$

By the same arguments, variational formulation (17b) is stable, that is,

$$\|\mathbf{u} - \mathbf{u}^h\|_{U(t)} \lesssim \|\nabla(r - r_h)\|. \quad (28)$$

An application of the triangle inequality (twice) and quasi-optimal convergence of (18a) prove that

$$\|\nabla r - \nabla r_h\| + \|\mathbf{u} - \mathbf{u}_h\|_{U(t)} \lesssim \|\nabla r - \nabla \tilde{r}_h\| + \|\mathbf{u} - \tilde{\mathbf{u}}_h\|_{U(t)} \quad \forall \tilde{r}_h \in P_u^{1,c}(\mathcal{T}), \tilde{\mathbf{u}}_h \in U_h(t).$$

This is (20). We proceed in the same way to bound  $\|\nabla(u - u_h)\|$ . Defining  $u^h \in H_u^1(\Omega)$  by

$$(\nabla u^h, \nabla \delta u) = t^2(f, \delta u) + (\boldsymbol{\psi}_h, \nabla \delta u) \quad \forall \delta u \in H_u^1(\Omega),$$

standard estimates (stability of (17c) by (6), Galerkin orthogonality of (18c), triangle inequality) imply that

$$\begin{aligned} \|\nabla(u^h - u_h)\| &\lesssim \|\nabla(u^h - \tilde{u}_h)\| \leq \|\nabla(u - u^h)\| + \|\nabla(u - \tilde{u}_h)\| \\ &\lesssim \|\boldsymbol{\psi} - \boldsymbol{\psi}_h\| + \|\nabla(u - \tilde{u}_h)\| \quad \forall \tilde{u}_h \in P_u^{1,c}(\mathcal{T}). \end{aligned} \quad (29)$$

Using again the triangle inequality and bounding  $\|\boldsymbol{\psi} - \boldsymbol{\psi}_h\| \leq \|\mathbf{u} - \mathbf{u}_h\|_{U(t)}$ , an application of the previous estimate (20) shows that (21) holds. This finishes the proof of Theorem 7.

### 4.3 Robust DPG scheme for large domains

Let us present the changes that are needed for our DPG scheme to be robust for larger domains, cf. Remark 1. We select a number  $d = d(\Omega) > 0$  so that the Korn and Poincaré inequalities

$$\|\boldsymbol{\chi}\|^2 + d^2 \|\nabla \boldsymbol{\chi}\|^2 \lesssim d^2 \|\boldsymbol{\varepsilon} \boldsymbol{\chi}\|^2 \quad \forall \boldsymbol{\chi} \in \mathbf{H}_\psi^1(\Omega), \quad \|v\|_* \lesssim d \|\nabla v\| \quad \forall v \in H_p^1(\Omega)$$

hold uniformly with respect to the diameter of  $\Omega$ . A standard choice is  $d = \text{diam}(\Omega)$ . We note that this tuning can be refined for an-isotropic domains, cf. [27]. Analogously to the definition of  $t_*$ , cf. (3), we introduce

$$d_* := 1 \quad \text{if } \Gamma_{\text{sc}} = \Gamma_{\text{sss}} = \emptyset \quad \text{and} \quad d_* := d \quad \text{if } \Gamma_{\text{sc}} \cup \Gamma_{\text{sss}} \neq \emptyset.$$

We then scale the norms as follows. In the test space we select

$$\begin{aligned} \|(\boldsymbol{\chi}, \boldsymbol{\rho})\|_{V_1(\mathcal{T},t)}^2 &:= d^{-2} \|\boldsymbol{\chi}\|^2 + \|\nabla \boldsymbol{\chi}\|_{\mathcal{T}}^2 + \|\boldsymbol{\rho}\|^2 + t^{-2} d^2 \|\text{rot}(t\boldsymbol{\rho} + \boldsymbol{\chi})\|_{\mathcal{T}}^2 && ((\boldsymbol{\chi}, \boldsymbol{\rho}) \in V_1(\mathcal{T})), \\ \|(\mathbf{S}, v)\|_{V_2(\mathcal{T},t)}^2 &:= \|\mathbf{S}\|^2 + t_*^2 d_*^{-2} \|v\|_*^2 + d^2 \|\text{div } \mathbf{S} - \text{curl } v\|_{\mathcal{T}}^2 + t^2 \|\text{curl } v\|_{\mathcal{T}}^2 && ((\mathbf{S}, v) \in V_2(\mathcal{T})). \end{aligned}$$

For the trace norms we re-scale the norms in  $U_1$  and  $U_2$  (cf. (13)) as

$$\begin{aligned} \|(\boldsymbol{\psi}, \boldsymbol{\eta})\|_{U_1(t)}^2 &:= d^{-2}\|\boldsymbol{\psi}\|^2 + \|\boldsymbol{\varepsilon}\boldsymbol{\psi}\|^2 + \|\boldsymbol{\eta}\|^2 + t_*^{-2}d_*^2\|\operatorname{rot}(t\boldsymbol{\eta} + \boldsymbol{\psi})\|^2 && ((\boldsymbol{\psi}, \boldsymbol{\eta}) \in U_1), \\ \|(\mathbf{M}, p)\|_{U_2(t)}^2 &:= \|\mathbf{M}\|^2 + t^2d^{-2}\|p\|_*^2 + d^2\|\operatorname{div} \mathbf{M} - \operatorname{curl} p\|^2 + t^2\|\operatorname{curl} p\|^2 && ((\mathbf{M}, p) \in U_2), \end{aligned}$$

and define norms  $\|\cdot\|_{\boldsymbol{\psi}, t}$  and  $\|\cdot\|_{M, t}$  in  $\mathbf{H}_0^\psi(\mathcal{S}, t)$  and  $\mathbf{H}_0^M(\mathcal{S}, t)$ , respectively, as in (15). Finally, the (squared) re-scaled norm in the trial space is

$$\|\mathbf{u}\|_{U(t)}^2 := d^{-2}\|\boldsymbol{\psi}\|^2 + \|\boldsymbol{\eta}\|^2 + \|\mathbf{M}\|^2 + t^2d^{-2}\|p\|_*^2 + \|\widehat{\boldsymbol{\psi}\boldsymbol{\eta}}\|_{\boldsymbol{\psi}, t}^2 + \|\widehat{M}p\|_{M, t}^2$$

for  $\mathbf{u} = (\boldsymbol{\psi}, \boldsymbol{\eta}, \mathbf{M}, p, \widehat{\boldsymbol{\psi}\boldsymbol{\eta}}, \widehat{M}p) \in U(t)$ , cf. (16), where the trace norms are the re-scaled ones.

All relations and estimates from Section 3 hold true uniformly with respect to the diameter of  $\Omega$ , when replacing the norms with the re-scaled ones just defined. In particular, the equality statements of Lemma 2 are valid. Furthermore, the stability statement from Proposition 9 becomes

$$\|(\boldsymbol{\chi}, \boldsymbol{\rho}, \mathbf{S}, v)\|_{V(\mathcal{T}, t)}^2 \lesssim d^2\|\mathbf{g}_1\|^2 + \|\mathbf{G}_2\|^2 + t^{-2}d^2\|\mathbf{g}_3\|^2 + \|\mathbf{g}_4\|^2.$$

Repeating the steps from §4.2 then shows the equivalence of norms

$$\|\cdot\|_{U(t)} \simeq \|B \cdot\|_{V(\mathcal{T}, t)'} \quad \text{in } U(t),$$

uniformly with respect to  $t \in (0, 1]$  and  $\operatorname{diam}(\Omega)$ .

Finally, with respect to the quasi-optimal error estimates, stage 1 of scheme (18) stays optimal in the  $H^1(\Omega)$ -seminorm. On the other hand, the estimate for stage 2 requires stability (28) which now renders

$$\|\mathbf{u} - \mathbf{u}^h\|_{U(t)}^2 \lesssim d^2\|\nabla(r - r_h)\|^2$$

due to the weighting  $d^{-1}\|\boldsymbol{\psi}\|$  of the norm of test-function component  $\boldsymbol{\psi}$  in (18b). We therefore have the a priori error estimates

$$\begin{aligned} \|\nabla(r - r_h)\|^2 &\lesssim \|\nabla(r - \tilde{r}_h)\|^2 && \forall \tilde{r}_h \in P_u^{1,c}(\mathcal{T}), \\ \|\mathbf{u} - \mathbf{u}_h\|_{U(t)}^2 &\lesssim d^2\|\nabla(r - \tilde{r}_h)\|^2 + \|\mathbf{u} - \tilde{\mathbf{u}}_h\|_{U(t)}^2 && \forall \tilde{r}_h \in P_u^{1,c}(\mathcal{T}), \tilde{\mathbf{u}}_h \in U_h(t). \end{aligned}$$

Proceeding as in (29), we obtain the error estimate for the third stage,

$$\begin{aligned} \|\nabla(u - u_h)\|^2 &\lesssim \|\boldsymbol{\psi} - \boldsymbol{\psi}_h\|^2 + \|\nabla(u - \tilde{u}_h)\|^2 \lesssim d^2\|\mathbf{u} - \mathbf{u}_h\|_{U(t)}^2 + \|\nabla(u - \tilde{u}_h)\|^2 \\ &\lesssim d^4\|\nabla(r - \tilde{r}_h)\|^2 + d^2\|\mathbf{u} - \tilde{\mathbf{u}}_h\|_{U(t)}^2 + \|\nabla(u - \tilde{u}_h)\|^2 \quad \forall \tilde{r}_h, \tilde{u}_h \in P_u^{1,c}(\mathcal{T}), \tilde{\mathbf{u}}_h \in U_h(t). \end{aligned}$$

These a priori error estimates for  $r, \mathbf{u}, u$  hold uniformly with respect to  $t \in (0, 1]$  and the diameter of  $\Omega$ .

## 5 Locking-free lowest-order discretization for hard-clamped plates

In order to prove our lowest-order scheme to be locking free, the solution must be sufficiently regular. Furthermore, to be able to use standard discrete spaces we restrict our analysis to the hard-clamped case. This is also the situation where regularity estimates are known. In the following,  $\|\cdot\|_m$  denotes the standard Sobolev norm in  $H^m(\Omega)$  ( $m = 1, 2$ ) for scalar, vector and tensor functions. Our assumption is the following.

**Assumption 11.** *We consider the hard-clamped case,  $\Gamma = \Gamma_{\text{hc}}$ . For given  $f \in L_2(\Omega)$  and  $t \in (0, 1]$ , let  $(\boldsymbol{\psi}, p) \in \mathbf{H}_0^1(\Omega) \times H^1(\Omega)$ ,  $r, u \in H_0^1(\Omega)$  denote the solution components of problems (7), (10), (11). We select  $p$  with  $(p, 1) = 0$ . The regularity estimate*

$$\|r\|_2 + \|u\|_2 + \|\boldsymbol{\psi}\|_2 + \|p\|_1 + t\|p\|_2 \lesssim \|f\|$$

holds true with a hidden constant that is independent of  $f$  and  $t$ .

For a special case, Arnold and Falk proved that this assumption is true. We note that this includes the case where, on the right-hand side of (17b),  $r$  is replaced with its conforming finite element approximation  $r_h$ .

**Proposition 12.** *[3, Theorem 2.1]*

*If  $\Omega$  is convex and  $\mathcal{C}$  is the identity tensor then Assumption 11 holds true.*

As previously specified in Section 4, we use regular triangular meshes which we now assume to be shape regular, and denote  $h := \max\{\text{diam}(T); T \in \mathcal{T}\}$ . We approximate  $H_0^1(\Omega)$  with continuous, piecewise linear polynomials, the space being denoted as  $P_0^{1,c}(\mathcal{T}) \subset H_0^1(\Omega)$ , as before. In the following we also need the piecewise polynomial space without boundary condition,  $P^{1,c}(\mathcal{T}) := P^1(\mathcal{T}) \cap H^1(\Omega)$ . We still have to specify the discrete subspace  $U_h(t) \subset U(t)$ . To this end, let  $\mathcal{RT}^0(\mathcal{T}) \subset \mathbf{H}(\text{div}, \Omega)$  and  $\mathcal{ND}^0(\mathcal{T}) \subset \mathbf{H}(\text{rot}, \Omega)$  denote the lowest-order Raviart–Thomas and Nédélec spaces, respectively. Of course,  $\mathcal{ND}^0(\mathcal{T})$  is a rotation of  $\mathcal{RT}^0(\mathcal{T})$ . Subspaces  $\mathcal{ND}_0^0(\mathcal{T}) \subset \mathbf{H}_0(\text{rot}, \Omega) \subset \mathbf{H}(\text{rot}, \Omega)$  denote the corresponding spaces of functions with zero tangential component on  $\Gamma$ . We define the discrete trace spaces

$$\begin{aligned} \mathbf{H}_h^\psi(\mathcal{S}, t) &:= \text{tr}^\psi \left( P_0^{1,c}(\mathcal{T})^2 \times \mathcal{ND}_0^0(\mathcal{T}) \right) \subset \mathbf{H}_0^\psi(\mathcal{S}, t), \\ \mathbf{H}_h^M(\mathcal{S}, t) &:= \text{tr}^M \left( \mathcal{RT}^0(\mathcal{T})^2 \times P^{1,c}(\mathcal{T}) \right) \subset \mathbf{H}_0^M(\mathcal{S}, t). \end{aligned}$$

Here,  $\mathcal{RT}^0(\mathcal{T})^2 \subset \mathbf{H}(\text{div}, \Omega)$  indicates that the Raviart–Thomas elements are taken row-wise. Recalling Remark 3, we note that  $\mathbf{H}_h^\psi(\mathcal{S}, t)$  consists of two components, one of continuous, piecewise linear vector functions on  $\mathcal{S}$ , and the second of piecewise constant functions on  $\mathcal{S}$ , plus homogeneous boundary conditions. Space  $\mathbf{H}_h^M(\mathcal{S}, t)$  also has two components, the first amounting to piecewise constant vector functions on  $\mathcal{S}$ , and the second to continuous, piecewise linear polynomials on  $\mathcal{S}$ . The field variables are approximated by piecewise constant functions. Therefore, the discrete approximation space for our DPG scheme (18b) is

$$U_h(t) := P^0(\mathcal{T})^2 \times P^0(\mathcal{T})^2 \times \left( P^0(\mathcal{T})^{2 \times 2} \cap \mathbb{L}_2^s(\Omega) \right) \times P^0(\mathcal{T}) \times \mathbf{H}_h^\psi(\mathcal{S}, t) \times \mathbf{H}_h^M(\mathcal{S}, t). \quad (30)$$



Under Assumption 11 the resulting DPG scheme is locking free, as stated next.

**Theorem 13.** *Suppose that Assumption 11 holds true. In particular, we consider the hard-clamped boundary condition. Furthermore, we assume that  $\mathcal{C}$  is a  $C^1$ -tensor. For  $f \in L_2(\Omega)$  and  $t \in (0, 1]$  let  $\mathbf{u} = (\boldsymbol{\psi}, \boldsymbol{\eta}, \mathbf{M}, p, \widehat{\boldsymbol{\psi}}\boldsymbol{\eta}, \widehat{\mathbf{M}}p) \in U(t)$  and  $u \in H_0^1(\Omega)$  denote the solutions of (17b) and (17c), respectively. Let  $\mathbf{u}_h = (\boldsymbol{\psi}_h, \boldsymbol{\eta}_h, \mathbf{M}_h, p_h, \widehat{\boldsymbol{\psi}}\boldsymbol{\eta}_h, \widehat{\mathbf{M}}p_h) \in U_h(t)$  and  $u_h \in P_0^{1,c}(\mathcal{T})$  be their corresponding approximations from (18b) and (18c). Using regular, shape-regular triangular meshes, the error estimate*

$$\|\nabla(u - u_h)\| + \|\boldsymbol{\psi} - \boldsymbol{\psi}_h\| + \|\mathbf{M} - \mathbf{M}_h\| \lesssim h\|f\|$$

holds true with a hidden constant that is independent of  $t$ ,  $f$ , and  $\mathcal{T}$ .

## 5.1 Proof of Theorem 13

We will employ some canonical approximation operators, recalled in the following together with their approximation properties.

- $\Pi_h^0 : L_2(\Omega) \rightarrow P^0(\mathcal{T})$  is the  $L_2(\Omega)$ -orthogonal projection onto piecewise constants with approximation property

$$\|(1 - \Pi_h^0)v\| \lesssim h\|v\|_1.$$

We use the same notation  $\Pi_h^0$  as component-wise application to vector or tensor functions.

- $\Pi_h^\nabla : L_2(\Omega) \rightarrow P_0^{1,c}(\mathcal{T})$  is a quasi-interpolation operator (Scott–Zhang) which satisfies

$$\|\Pi_h^\nabla v\| \lesssim \|v\|, \quad \|\Pi_h^\nabla v\|_1 \lesssim \|v\|_1, \quad h^{-1}\|(1 - \Pi_h^\nabla)v\| + \|(1 - \Pi_h^\nabla)v\|_1 \lesssim h\|v\|_2.$$

We use the same notation  $\Pi_h^\nabla$  as component-wise application to vector functions.

- $\Pi_h^{\text{div}} : \mathbf{H}(\text{div}, \Omega) \rightarrow \mathcal{RT}^0(\mathcal{T})$  is the interpolation operator introduced by Ern *et al.* [25, Section 3.1]. It satisfies

$$\begin{aligned} \|\Pi_h^{\text{div}} \boldsymbol{\phi}\| &\lesssim \|\boldsymbol{\phi}\| + h\|(1 - \Pi_h^0)\text{div} \boldsymbol{\phi}\|, & \|(1 - \Pi_h^{\text{div}})\boldsymbol{\phi}\| &\lesssim h\|\boldsymbol{\phi}\|_1, \\ \text{div}(1 - \Pi_h^{\text{div}})\boldsymbol{\phi} &= (1 - \Pi_h^0)\text{div} \boldsymbol{\phi}. \end{aligned}$$

We use the same notation  $\Pi_h^{\text{div}}$  as row-wise application to tensor functions.

- $\Pi_h^{\text{rot}} : \mathbf{H}_0(\text{rot}, \Omega) \rightarrow \mathcal{ND}_0^0(\mathcal{T})$  is the rotated version of  $\Pi_h^{\text{div}}$ , mapping to the Nédélec space of rotated Raviart–Thomas elements, and including the boundary condition of zero tangential components on  $\Gamma$ . Operator  $\Pi_h^{\text{rot}}$  has the same approximation properties as  $\Pi_h^{\text{div}}$ , replacing  $\text{div}$  with  $\text{rot}$ .

Now, in order to prove Theorem 13, it suffices to bound the right-hand side from (21) for appropriately selected discrete functions  $\tilde{r}_h, \tilde{u}_h \in P_0^{1,c}(\mathcal{T})$ ,  $\tilde{\mathbf{u}}_h = (\boldsymbol{\phi}_h, \boldsymbol{\xi}_h, \mathbf{N}_h, q_h, \widehat{\boldsymbol{\phi}}\boldsymbol{\xi}_h, \widehat{\mathbf{N}}q_h) \in U_h(t)$ .

1. Regularity. Recall the regularity properties from Assumption 11 where we include the replacement of  $r$  with  $r_h$  in (10a) and (18b), and select  $p$  with  $(p, 1) = 0$ . Since  $\mathcal{C}$  is  $C^1$  by assumption, relations  $\mathbf{M} = -\mathcal{C}\boldsymbol{\varepsilon}\boldsymbol{\psi}$  and  $\boldsymbol{\eta} = t \mathbf{curl} p$  imply that

$$\|r\|_2 + \|u\|_2 + \|\boldsymbol{\psi}\|_2 + \|p\|_1 + t\|p\|_2 + \|\mathbf{M}\|_1 + \|\boldsymbol{\eta}\|_1 \lesssim \|f\|.$$

This regularity will be used throughout in the following.

2. Approximation of  $r$  and  $u$ . We define  $\tilde{r}_h := \Pi_h^\nabla r$  and  $\tilde{u}_h = \Pi_h^\nabla u$ . This gives

$$\|\nabla(r - \tilde{r}_h)\| + \|\nabla(u - \tilde{u}_h)\| \lesssim h\|f\|.$$

3. Approximation of the field variables from  $\mathbf{u}$ . We choose

$$\boldsymbol{\phi}_h := \Pi_h^0 \boldsymbol{\psi}, \quad \boldsymbol{\xi}_h := \Pi_h^0 \boldsymbol{\eta}, \quad \mathbf{N}_h := \Pi_h^0 \mathbf{M}, \quad q_h := \Pi_h^0 p.$$

The approximation properties of  $\Pi_h^0$  show that

$$\|\boldsymbol{\psi} - \boldsymbol{\phi}_h\| + \|\boldsymbol{\eta} - \boldsymbol{\xi}_h\| + \|\mathbf{M} - \mathbf{N}_h\| + \|p - q_h\| \lesssim h(\|\boldsymbol{\psi}\|_1 + \|\boldsymbol{\eta}\|_1 + \|\mathbf{M}\|_1 + \|p\|_1) \lesssim h\|f\|.$$

4. Approximation of trace  $\widehat{\boldsymbol{\psi}}\boldsymbol{\eta}$ . We select

$$\widehat{\boldsymbol{\xi}}_h := \text{tr}^\psi(\Pi_h^\nabla \boldsymbol{\psi}, \Pi_h^{\text{rot}} \boldsymbol{\eta}).$$

By definition of trace operator  $\text{tr}^\psi$  we find that, for  $(\mathbf{S}, v) \in V_2(\mathcal{T})$ ,

$$\begin{aligned} \langle \widehat{\boldsymbol{\psi}}\boldsymbol{\eta} - \widehat{\boldsymbol{\xi}}_h, (\mathbf{S}, v) \rangle_{\mathcal{S}} &= ((1 - \Pi_h^\nabla) \boldsymbol{\psi}, \mathbf{div} \mathbf{S} - \mathbf{curl} v)_{\mathcal{T}} - ((1 - \Pi_h^{\text{rot}}) \boldsymbol{\eta}, t \mathbf{curl} v)_{\mathcal{T}} \\ &\quad + (\boldsymbol{\varepsilon}(1 - \Pi_h^\nabla) \boldsymbol{\psi}, \mathbf{S})_{\mathcal{T}} + (\text{rot}(t(1 - \Pi_h^{\text{rot}}) \boldsymbol{\eta} + (1 - \Pi_h^\nabla) \boldsymbol{\psi}), v)_{\mathcal{T}}. \end{aligned}$$

Bounding the terms involving  $(1 - \Pi_h^\nabla) \boldsymbol{\psi}$  shows that

$$\begin{aligned} &|((1 - \Pi_h^\nabla) \boldsymbol{\psi}, \mathbf{div} \mathbf{S} - \mathbf{curl} v)_{\mathcal{T}}| + |(\boldsymbol{\varepsilon}(1 - \Pi_h^\nabla) \boldsymbol{\psi}, \mathbf{S})_{\mathcal{T}}| + |(\text{rot}(1 - \Pi_h^\nabla) \boldsymbol{\psi}, v)_{\mathcal{T}}| \\ &\lesssim \|(1 - \Pi_h^\nabla) \boldsymbol{\psi}\| \|\mathbf{div} \mathbf{S} - \mathbf{curl} v\| + \|\boldsymbol{\varepsilon}(1 - \Pi_h^\nabla) \boldsymbol{\psi}\| \|\mathbf{S}\| + \|\text{rot}(1 - \Pi_h^\nabla) \boldsymbol{\psi}\| \|v\|_* \\ &\lesssim h\|\boldsymbol{\psi}\|_2 \|(\mathbf{S}, v)\|_{V_2(\mathcal{T}, t)} \lesssim h\|f\| \|(\mathbf{S}, v)\|_{V_2(\mathcal{T}, t)}. \end{aligned}$$

For the remaining terms we use the commutativity property  $\text{rot}(1 - \Pi_h^{\text{rot}}) \boldsymbol{\eta} = (1 - \Pi_h^0) \text{rot} \boldsymbol{\eta}$ . This yields

$$\begin{aligned} &|((1 - \Pi_h^{\text{rot}}) \boldsymbol{\eta}, t \mathbf{curl} v)_{\mathcal{T}}| + t|(\text{rot}(1 - \Pi_h^{\text{rot}}) \boldsymbol{\eta}, v)_{\mathcal{T}}| \\ &= |((1 - \Pi_h^{\text{rot}}) \boldsymbol{\eta}, t \mathbf{curl} v)_{\mathcal{T}}| + t|((1 - \Pi_h^0) \text{rot} \boldsymbol{\eta}, v)_{\mathcal{T}}| \\ &= |((1 - \Pi_h^{\text{rot}}) \boldsymbol{\eta}, t \mathbf{curl} v)_{\mathcal{T}}| + t|(\text{rot} \boldsymbol{\eta}, (1 - \Pi_h^0) v)_{\mathcal{T}}| \\ &\lesssim h\|\boldsymbol{\eta}\|_1 t \|\mathbf{curl} v\|_{\mathcal{T}} + h\|\boldsymbol{\eta}\|_1 t \|\nabla v\|_{\mathcal{T}} \lesssim h\|f\| \|(\mathbf{S}, v)\|_{V_2(\mathcal{T}, t)}. \end{aligned}$$

Here, we also used that  $\|\nabla v\|_{\mathcal{T}} = \|\mathbf{curl} v\|_{\mathcal{T}}$ .

5. Approximation of trace  $\widehat{M}p$ . We select  $q_h := \Pi_h^\nabla p$ ,  $\mathbf{N}_h := \Pi_h^{\text{div}}(\mathbf{M} - R(p - q_h))$  with

$$R = \begin{pmatrix} 0 & 1 \\ -1 & 0 \end{pmatrix}$$

so that  $\mathbf{div} R(\cdot) = \mathbf{curl}(\cdot)$ . Since  $p - q_h \in H^1(\Omega)$  we have that  $R(p - q_h) \in \mathbf{H}(\mathbf{div}, \Omega)$ . Then we define

$$\widehat{N}q_h := \text{tr}^M(\mathbf{N}_h, q_h).$$

By definition of trace operator  $\text{tr}^M$  we find that, for  $(\boldsymbol{\chi}, \boldsymbol{\rho}) \in V_1(\mathcal{T})$ ,

$$\begin{aligned} \langle \widehat{M}p - \widehat{N}q_h, (\boldsymbol{\chi}, \boldsymbol{\rho}) \rangle_S &= (\mathbf{div}(\mathbf{M} - \mathbf{N}_h) - \mathbf{curl}(p - q_h), \boldsymbol{\chi})_{\mathcal{T}} - (t \mathbf{curl}(p - q_h), \boldsymbol{\rho})_{\mathcal{T}} \\ &\quad + (\mathbf{M} - \mathbf{N}_h, \boldsymbol{\varepsilon}\boldsymbol{\chi})_{\mathcal{T}} + (p - q_h, \text{rot}(t\boldsymbol{\rho} + \boldsymbol{\chi}))_{\mathcal{T}}. \end{aligned}$$

We bound

$$\begin{aligned} |(t \mathbf{curl}(p - q_h), \boldsymbol{\rho})_{\mathcal{T}}| + |(p - q_h, \text{rot}(t\boldsymbol{\rho} + \boldsymbol{\chi}))_{\mathcal{T}}| \\ \lesssim ht \|p\|_2 \|\boldsymbol{\rho}\| + th^2 \|p\|_2 t^{-1} \|\text{rot}(t\boldsymbol{\rho} + \boldsymbol{\chi})\|_{\mathcal{T}} \lesssim h \|f\| \|(\boldsymbol{\chi}, \boldsymbol{\rho})\|_{V_1(\mathcal{T}, t)}. \end{aligned}$$

The term  $(\mathbf{M} - \mathbf{N}_h, \boldsymbol{\varepsilon}\boldsymbol{\chi})_{\mathcal{T}}$  is straightforward to bound. Using the properties of  $\Pi_h^{\text{div}}$ ,  $\Pi_h^\nabla$ , and noting that  $(1 - \Pi_h^0)\mathbf{div} Rq_h = 0$  since  $q_h$  is piecewise affine, we obtain

$$\begin{aligned} |(\mathbf{M} - \mathbf{N}_h, \boldsymbol{\varepsilon}\boldsymbol{\chi})_{\mathcal{T}}| &\lesssim \|\mathbf{M} - \mathbf{N}_h\| \|\boldsymbol{\varepsilon}\boldsymbol{\chi}\|_{\mathcal{T}} \lesssim (\|\mathbf{M} - \Pi_h^{\text{div}} \mathbf{M}\| + \|\Pi_h^{\text{div}} R(p - q_h)\|) \|(\boldsymbol{\chi}, \boldsymbol{\rho})\|_{V_1(\mathcal{T}, t)} \\ &\lesssim (h \|\mathbf{M}\|_1 + \|p - q_h\| + h \|(1 - \Pi_h^0)\mathbf{div} R(p - q_h)\|) \|(\boldsymbol{\chi}, \boldsymbol{\rho})\|_{V_1(\mathcal{T}, t)} \\ &\lesssim h (\|\mathbf{M}\|_1 + \|p\|_1 + \|(1 - \Pi_h^0)\mathbf{curl} p\|) \|(\boldsymbol{\chi}, \boldsymbol{\rho})\|_{V_1(\mathcal{T}, t)} \\ &\leq h (\|\mathbf{M}\|_1 + \|p\|_1 + \|\mathbf{curl} p\|) \|(\boldsymbol{\chi}, \boldsymbol{\rho})\|_{V_1(\mathcal{T}, t)} \lesssim h \|f\| \|(\boldsymbol{\chi}, \boldsymbol{\rho})\|_{V_1(\mathcal{T}, t)}. \end{aligned}$$

For the final term of the approximation of  $\widehat{M}p$  we note that, by construction of  $\mathbf{N}_h$ ,

$$\begin{aligned} \mathbf{div}(\mathbf{M} - \mathbf{N}_h) - \mathbf{curl}(p - q_h) &= \mathbf{div}(1 - \Pi_h^{\text{div}})\mathbf{M} - \mathbf{div}(1 - \Pi_h^{\text{div}})R(p - q_h) \\ &= \mathbf{div}(1 - \Pi_h^{\text{div}})(\mathbf{M} - R(p - q_h)) = (1 - \Pi_h^0)\mathbf{div}(\mathbf{M} - R(p - q_h)) \\ &= (1 - \Pi_h^0)\mathbf{div}(\mathbf{M} - Rp) = (1 - \Pi_h^0)(\mathbf{div} \mathbf{M} - \mathbf{curl} p). \end{aligned}$$

Recall from (10a) that  $\mathbf{div} \mathbf{M} - \mathbf{curl} p = \nabla r$  with  $r \in H_0^1(\Omega)$  being the solution to Poisson problem (17a). Therefore,

$$\begin{aligned} |(\mathbf{div}(\mathbf{M} - \mathbf{N}_h) - \mathbf{curl}(p - q_h), \boldsymbol{\chi})_{\mathcal{T}}| &= |((1 - \Pi_h^0)\nabla r, \boldsymbol{\chi})| = |((1 - \Pi_h^0)\nabla r, (1 - \Pi_h^0)\boldsymbol{\chi})| \\ &\lesssim h^2 \|r\|_2 \|\boldsymbol{\chi}\|_1 \lesssim h^2 \|f\| \|(\boldsymbol{\chi}, \boldsymbol{\rho})\|_{V_1(\mathcal{T}, t)}. \end{aligned}$$

Note that this term is of higher order.

Collecting all the estimates this concludes the proof of Theorem 13.

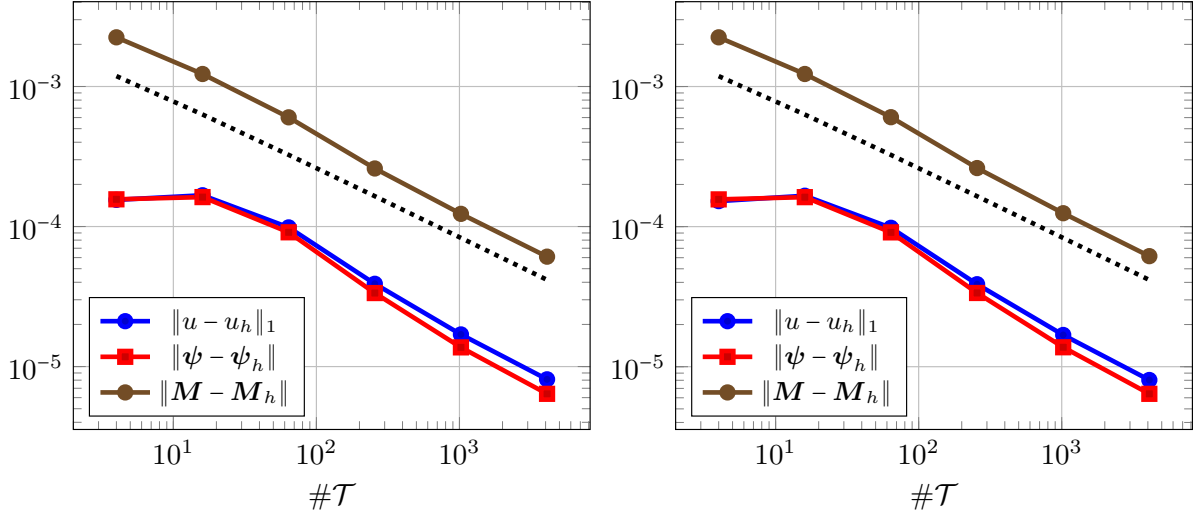


Figure 1: Errors for the polynomial solution from Section 6.1 with  $t = 10^{-2}$  (left) and  $t = 10^{-4}$  (right). Dashed black lines indicate  $\mathcal{O}(\#\mathcal{T}^{-1/2})$ .

## 6 Numerical experiments

Throughout we consider the scaled Reissner–Mindlin model (2) with identity tensor  $\mathcal{C}$ . We study four problems and their numerical solution by the three-stage scheme (18) where discrete space  $U_h$  is selected as in (30), with boundary conditions as needed. As noted in Remark 8(i), trial-to-test operator  $\mathfrak{T}$  from (19) has to be approximated. For all the examples we do this by solving (19) in the piecewise polynomial (degree 3) subspace of  $V(\mathcal{T})$ , rather than in  $V(\mathcal{T})$ . In three of the four cases, the exact solutions are known and we report on the approximation errors  $\|u - u_h\|_1$ ,  $\|\psi - \psi_h\|$ , and  $\|\mathbf{M} - \mathbf{M}_h\|$  (recall that  $\|\cdot\|_1$  refers to the standard  $H^1(\Omega)$ -norm). Specifically, Problem 1 is that of a polynomial solution with hard-clamped boundary and has been used in several publications before, Problem 2 is derived from the Kirchhoff solution and has hard simple support, for Problem 3 we consider a non-convex polygon with a combination of clamped and free boundary pieces, and Problem 4 stems from Di Pietro and Droniou [24] and has a  $t$ -dependent regularity (we use the corresponding non-homogeneous hard-clamped condition).

Problem 1 satisfies our conditions from Section 5 that guarantee that our method is locking free. We don't have an exact solution of Problem 3. In that case we plot the a posteriori error estimators. The numerical results indicate the absence of locking for all the problems studied here.

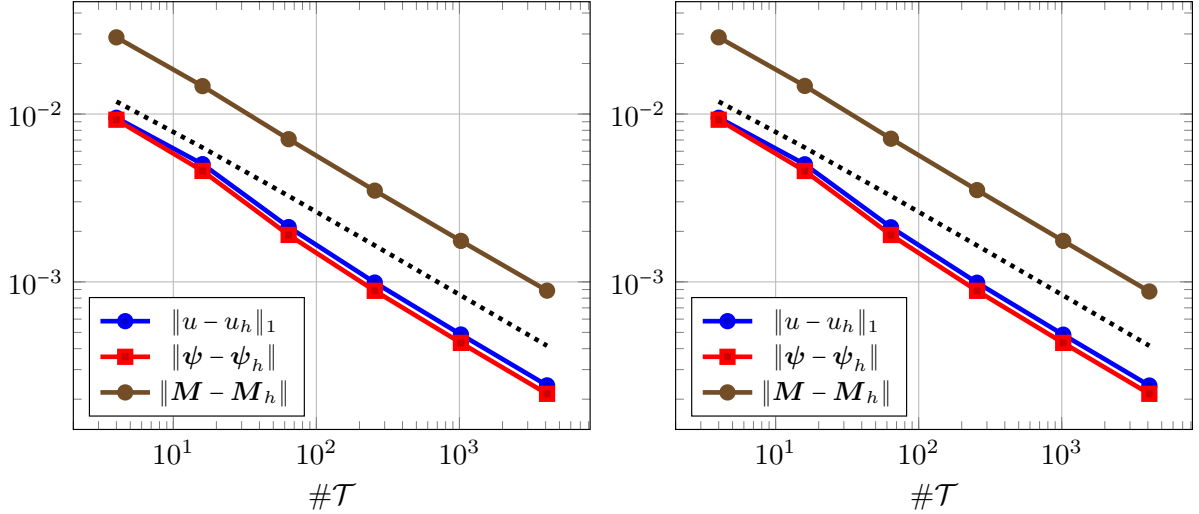


Figure 2: Errors for example with Kirchhoff solution and hard simple support from Section 6.2, with  $t = 10^{-2}$  (left) and  $t = 10^{-4}$  (right). Dashed black lines indicate  $\mathcal{O}(\#\mathcal{T}^{-1/2})$ .

### 6.1 Example with polynomial solution

We consider domain  $\Omega = (0, 1)^2$  and a manufactured polynomial solution. Starting with

$$\psi(x, y) = \begin{pmatrix} y^3(y-1)^3x^2(x-1)^2(2x-1) \\ x^3(x-1)^3y^2(y-1)^2(2y-1) \end{pmatrix},$$

we calculate  $\mathbf{M} = -\varepsilon\psi$ , and  $u \in H_0^1(\Omega)$  can be obtained from relation  $\nabla u = t^2 \operatorname{div} \mathbf{M} + \psi$ . This solution satisfies the hard-clamped boundary condition.

Figure 1 shows the errors for plate thickness parameter  $t = 10^{-2}$  (left plot) and  $t = 10^{-4}$  (right plot), using a sequence of uniformly refined meshes. As shown in Section 5, our method is locking free in this case. The numerical results confirm our result.

### 6.2 Example with hard simple support

In this example we select  $\Omega = (0, 1)^2$ . Let  $u_K$  be the Kirchhoff solution defined by

$$\Delta^2 u_K = 1 \quad \text{in } \Omega, \quad u_K = \Delta u_K = 0 \quad \text{on } \Gamma.$$

It can be represented as the Fourier series

$$u_K(x, y) = \sum_{n,m=1}^{\infty} \frac{4(1 - \cos(m\pi))(1 - \cos(n\pi))}{\pi^6 mn(m^2 + n^2)^2} \sin(m\pi x) \sin(n\pi y).$$

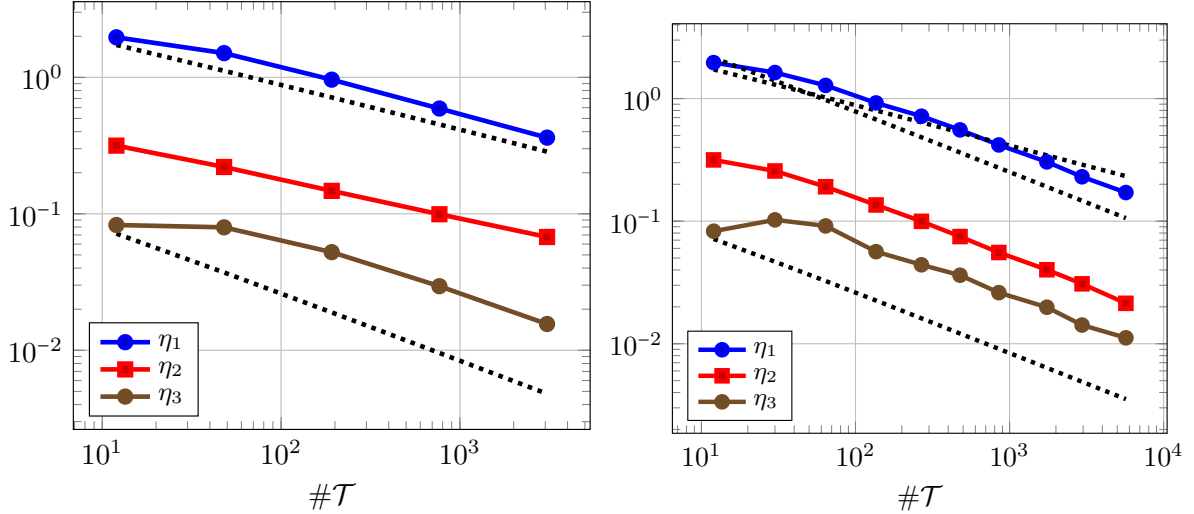


Figure 3: Errors for example with singular solution from Section 6.2 and  $t = 10^{-3}$ , uniform (left) and adaptively refined meshes (right). Dashed black lines indicate  $\mathcal{O}(\#\mathcal{T}^{-1/3})$  or  $\mathcal{O}(\#\mathcal{T}^{-1/2})$ .

Defining

$$u = u_K - t^2 \Delta u_K, \quad \psi = \nabla u_K, \quad \mathbf{M} = -\varepsilon \psi, \quad \mathbf{q} = -\nabla \Delta u_K$$

one verifies that this gives a solution of (2) with  $\mathcal{C} = \text{id}$ ,  $f = -\text{div } \mathbf{q} = 1$ , and hard simple support. To calculate approximation errors, we replace  $u_K$  by its first  $200^2$  Fourier terms.

Figure 2 shows the errors for  $t = 10^{-2}$  (left plot) and  $t = 10^{-4}$  (right plot), using a sequence of uniformly refined meshes. We observe that our results appear to be locking free also for this case with hard simple support.

### 6.3 Example with singular solution

We consider the L-shaped domain  $\Omega = (-1, 1)^2 \setminus [-1, 0]^2$  and constant load  $f = 1$ . The edges adjacent to the origin are hard clamped and all the others are free. The exact solution to this problem is unknown, and due to the incoming corner we expect the solution to have a corner singularity of reduced regularity. Therefore, our method should exhibit a reduced order of convergence when using quasi-uniform meshes. It is natural to consider adaptive mesh refinements to regain the optimal convergence rate. To do so, we use a simple a posteriori error estimator composed of an estimator for each of the three stages, written as

$$\eta^2 := \eta_1^2 + \eta_2^2 + \eta_3^2.$$

Estimator  $\eta_2$  denotes the built-in error estimator of the DPG method, cf. [19] for details, and  $\eta_1$ ,  $\eta_3$  are weighted residual Poisson estimators, see, e.g., [1, Chapter 2]. All these estimators are

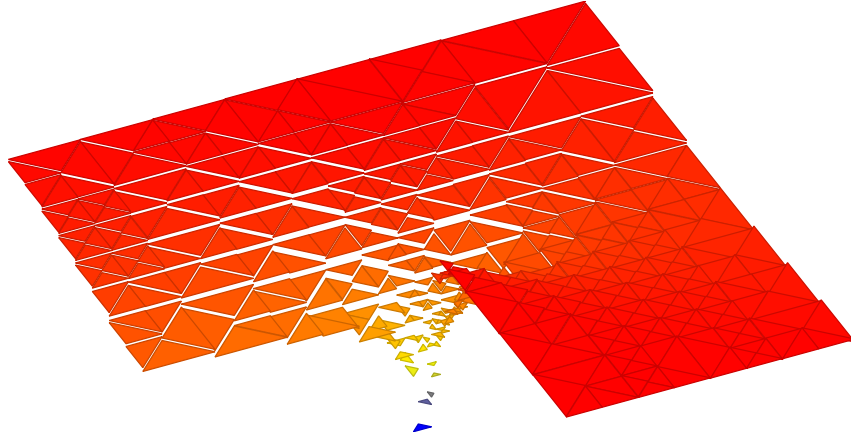


Figure 4: Approximation of bending moment  $\mathbf{M}_{22}$  on adaptively refined mesh ( $\#\mathcal{T} = 477$ ) from the example with singular solution in Section 6.3.

localizable with respect to the elements of the mesh,  $\eta_j^2 = \sum_{T \in \mathcal{T}} \eta_j(T)^2$ , and thus can be used to steer a standard adaptive algorithm. We use the bulk criterion

$$\frac{1}{2}\eta^2 \leq \sum_{T \in \mathcal{M}} \eta^2(T)$$

to mark elements and newest-vertex bisection for mesh refinement. Here,  $\mathcal{M}$  denotes a (minimal) set of elements marked for refinement.

Figure 3 shows the three error estimators on a sequence of uniformly (left plot) and adaptively refined meshes (right plot). As expected, for uniform meshes we observe a reduced convergence rate whereas the optimal rate is recovered through adaptivity. The presented results are for  $t = 10^{-3}$  and, interestingly, we do not observe any locking effect.

Figure 4 shows component  $\mathbf{M}_{22}$  of the bending moment approximation on an adaptively refined mesh. It seems to behave singularly at the incoming corner, as do the other components (not shown).

#### 6.4 Example with $t$ -dependent behavior

We consider the manufactured solution from Di Pietro and Droniou [24], with domain  $\Omega = (0, 1)^2$ . We only note that in this case the  $H^1(\Omega)$ -norm of the shear force depends on  $t$  and blows up like  $t^{-1/2}$ , whereas  $\operatorname{div} \mathbf{q} = -f$  is independent of  $t$ . We refer to [24, Section 5.2.1] for details on the precise construction, cf. also [4]. We impose hard-clamped boundary conditions and note that they are non-homogeneous.

Figure 5 shows the errors for  $t = 10^{-2}$  (left plot) and  $t = 10^{-4}$  (right plot), using a sequence of uniformly refined meshes. Again, we observe that our results are locking free.

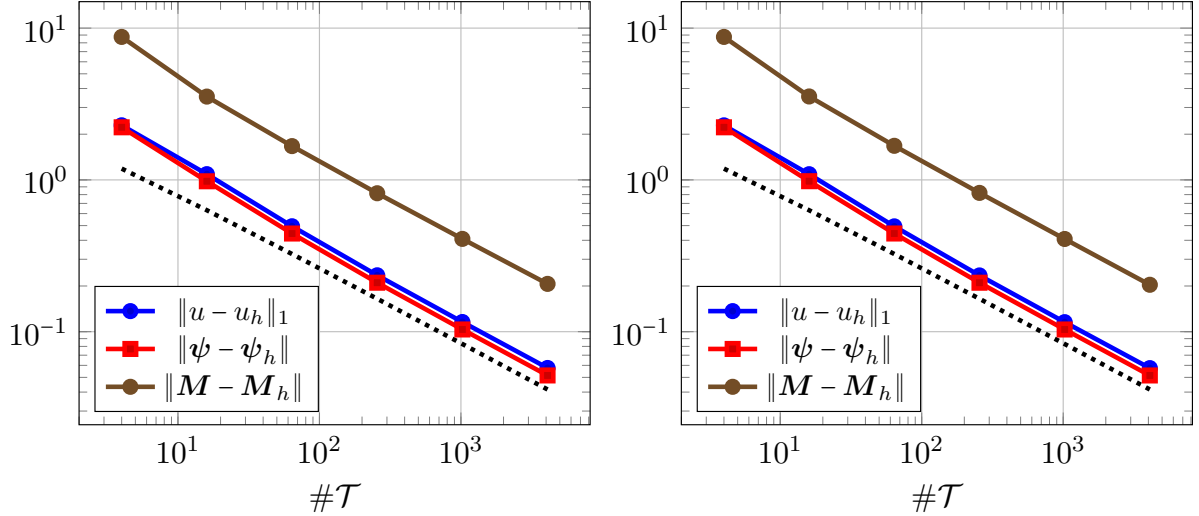


Figure 5: Errors for example with  $t$ -dependent solution from Section 6.4 with  $t = 10^{-2}$  (left) and  $t = 10^{-4}$  (right). Dashed black lines indicate  $\mathcal{O}(\#\mathcal{T}^{-1/2})$ .

## References

- [1] M. AINSWORTH AND J. T. ODEN, *A posteriori error estimation in finite element analysis*, Wiley, 2000.
- [2] D. N. ARNOLD, F. BREZZI, R. S. FALK, AND L. D. MARINI, *Locking-free Reissner-Mindlin elements without reduced integration*, *Comput. Methods Appl. Mech. Engrg.*, 196 (2007), pp. 3660–3671.
- [3] D. N. ARNOLD AND R. S. FALK, *A uniformly accurate finite element method for the Reissner-Mindlin plate*, *SIAM J. Numer. Anal.*, 26 (1989), pp. 1276–1290.
- [4] —, *Asymptotic analysis of the boundary layer for the Reissner-Mindlin plate model*, *SIAM J. Math. Anal.*, 27 (1996), pp. 486–514.
- [5] —, *Analysis of a linear-linear finite element for the Reissner-Mindlin plate model*, *Math. Models Methods Appl. Sci.*, 7 (1997), pp. 217–238.
- [6] D. N. ARNOLD, L. R. SCOTT, AND M. VOGELIUS, *Regular inversion of the divergence operator with Dirichlet boundary conditions on a polygon*, *Ann. Scuola Norm. Sup. Pisa Cl. Sci. (4)*, 15 (1988), pp. 169–192 (1989).
- [7] C. BACUTA, L. DEMKOWICZ, J. MORA, AND C. XENOPHONTOS, *Analysis of non-conforming DPG methods on polyhedral meshes using fractional Sobolev norms*, *Comput. Math. Appl.*, 95 (2021), pp. 215–241.



- [8] L. BEIRÃO DA VEIGA, D. MORA, AND G. RIVERA, *Virtual elements for a shear-deflection formulation of Reissner-Mindlin plates*, *Math. Comp.*, 88 (2019), pp. 149–178.
- [9] P. R. BÖSING AND C. CARSTENSEN, *Discontinuous Galerkin with weakly over-penalized techniques for Reissner-Mindlin plates*, *J. Sci. Comput.*, 64 (2015), pp. 401–424.
- [10] ———, *Weakly over-penalized discontinuous Galerkin schemes for Reissner-Mindlin plates without the shear variable*, *Numer. Math.*, 130 (2015), pp. 395–423.
- [11] J. H. BRAMBLE AND T. SUN, *A negative-norm least squares method for Reissner-Mindlin plates*, *Math. Comp.*, 67 (1998), pp. 901–916.
- [12] F. BREZZI, K.-J. BATHE, AND M. FORTIN, *Mixed-interpolated elements for Reissner-Mindlin plates*, *Internat. J. Numer. Methods Engrg.*, 28 (1989), pp. 1787–1801.
- [13] F. BREZZI AND M. FORTIN, *Numerical approximation of Mindlin-Reissner plates*, *Math. Comp.*, 47 (1986), pp. 151–158.
- [14] F. BREZZI, M. FORTIN, AND R. STENBERG, *Error analysis of mixed-interpolated elements for Reissner-Mindlin plates*, *Math. Models Methods Appl. Sci.*, 1 (1991), pp. 125–151.
- [15] P. BRINGMANN AND C. CARSTENSEN,  *$h$ -adaptive least-squares finite element methods for the 2D Stokes equations of any order with optimal convergence rates*, *Comput. Math. Appl.*, 74 (2017), pp. 1923–1939.
- [16] Z. CAI, *Least squares for the perturbed Stokes equations and the Reissner-Mindlin plate*, *SIAM J. Numer. Anal.*, 38 (2000), pp. 1561–1581.
- [17] Z. CAI, X. YE, AND H. ZHANG, *Least-squares finite element approximations for the Reissner-Mindlin plate*, *Numer. Linear Algebra Appl.*, 6 (1999), pp. 479–496. Iterative solution methods for the elasticity equations in mechanics and biomechanics, IMMB’98, Part 1 (Nijmegen).
- [18] V. M. CALO, N. O. COLLIER, AND A. H. NIEMI, *Analysis of the discontinuous Petrov-Galerkin method with optimal test functions for the Reissner-Mindlin plate bending model.*, *Comput. Math. Appl.*, 66 (2014), pp. 2570–2586.
- [19] C. CARSTENSEN, L. F. DEMKOWICZ, AND J. GOPALAKRISHNAN, *A posteriori error control for DPG methods*, *SIAM J. Numer. Anal.*, 52 (2014), pp. 1335–1353.
- [20] ———, *Breaking spaces and forms for the DPG method and applications including Maxwell equations*, *Comput. Math. Appl.*, 72 (2016), pp. 494–522.
- [21] L. F. DEMKOWICZ AND J. GOPALAKRISHNAN, *A class of discontinuous Petrov-Galerkin methods. Part II: Optimal test functions*, *Numer. Methods Partial Differential Eq.*, 27 (2011), pp. 70–105.

- [22] ———, *An overview of the discontinuous Petrov Galerkin method*, in Recent developments in discontinuous Galerkin finite element methods for partial differential equations, vol. 157 of IMA Vol. Math. Appl., Springer, Cham, 2014, pp. 149–180.
- [23] L. F. DEMKOWICZ, J. GOPALAKRISHNAN, AND A. H. NIEMI, *A class of discontinuous Petrov-Galerkin methods. Part III: Adaptivity*, Appl. Numer. Math., 62 (2012), pp. 396–427.
- [24] D. A. DI PIETRO AND J. O. DRONIOU, *A DDR method for the Reissner–Mindlin plate bending problem on polygonal meshes*, arXiv 2105.11773, 2021.
- [25] A. ERN, T. GUDI, I. SMEARS, AND M. VOHRALÍK, *Equivalence of local- and global-best approximations, a simple stable local commuting projector, and optimal hp approximation estimates in  $H(\text{div})$* , IMA J. Numer. Anal. online, <https://doi.org/10.1093/imanum/draa103>.
- [26] T. FÜHRER AND N. HEUER, *Fully discrete DPG methods for the Kirchhoff–Love plate bending model*, Comput. Methods Appl. Mech. Engrg., 343 (2019), pp. 550–571.
- [27] ———, *A robust DPG method for large domains*, Comput. Math. Appl., 94 (2021), pp. 15–27.
- [28] T. FÜHRER, N. HEUER, AND A. H. NIEMI, *An ultraweak formulation of the Kirchhoff–Love plate bending model and DPG approximation*, Math. Comp., 88 (2019), pp. 1587–1619.
- [29] ———, *A DPG method for shallow shells*, arXiv 2107.07624, 2021.
- [30] T. FÜHRER, N. HEUER, AND F.-J. SAYAS, *An ultraweak formulation of the Reissner–Mindlin plate bending model and DPG approximation*, Numer. Math., 145 (2020), pp. 313–344.
- [31] J. GOPALAKRISHNAN AND W. QIU, *An analysis of the practical DPG method*, Math. Comp., 83 (2014), pp. 537–552.